

Superheavy nuclei in relativistic effective Lagrangian model

Tapas Sil¹, S. K. Patra², B. K. Sharma², M. Centelles¹, and X. Viñas¹

¹*Departament d'Estructura i Constituents de la Matèria, Facultat de Física,*

Universitat de Barcelona, Diagonal 647, 08028 Barcelona, Spain

²*Institute of Physics, Sachivalaya Marg, Bhubaneswar 751 005, India.*

Abstract

Isotopic and isotonic chains of superheavy nuclei are analyzed to search for spherical double shell closures beyond $Z = 82$ and $N = 126$ within the new effective field theory model of Furnstahl, Serot, and Tang for the relativistic nuclear many-body problem. We take into account several indicators to identify the occurrence of possible shell closures, such as two-nucleon separation energies, two-nucleon shell gaps, average pairing gaps, and the shell correction energy. We also discuss some features of the particle densities and spin-orbit potentials of selected nuclei in the superheavy region. The effective Lagrangian model predicts $N = 172$ and $Z = 120$ and $N = 258$ and $Z = 120$ as stable spherical doubly magic superheavy nuclei, whereas $N = 184$ and $Z = 114$ show some magic character depending on the parameter set. The magicity of a particular neutron (proton) number in the analyzed mass region is found to depend on the number of protons (neutrons) present in the nucleus.

Keywords: Superheavy elements, binding energies, shell structure, relativistic mean field, effective field theory

PACS number(s): 21.60.-n, 21.10.Dr, 21.30.Fe, 27.90.+b

Typeset using REVTeX

I. INTRODUCTION

In the last thirty years a continuing effort has been devoted to the investigation of superheavy nuclei both in experiments and in theoretical research. A fascinating challenge in the study of these nuclei is the quest for the islands of stability where the next magic numbers beyond $N = 126$ and $Z = 82$ may be located. Experiments made at GSI, Dubna and Berkeley have allowed the synthesis and detection of some superheavy nuclei. For instance, light isotopes of the elements $Z = 110$ – 112 were obtained at GSI and Dubna [1–3]. These new elements were identified by their α -decay chains which lead to already known isotopes. Data of some heavier and neutron-richer isotopes of $Z = 112$, 114 and 116 produced by means of fusion reactions have been measured at Dubna [4].

Theoretical predictions made at the end of the sixties pointed towards the existence of an island of long-lived superheavy elements (SHE) centered around $N = 184$ and $Z = 114$ [5–8]. Such SHE with $Z > 100$, having a negligible liquid-drop fission barrier, would be stabilised mostly by quantal shell effects. Many of the more recent theoretical works on superheavy nuclei are based on the nuclear mean field approach and can be classified in two main groups. On the one hand, we have the self-consistent Hartree-Fock or Hartree calculations using Skyrme forces or the relativistic non-linear $\sigma - \omega$ model, respectively. On the other hand, there are the macroscopic-microscopic models which include a liquid-drop contribution for the part of the energy which varies smoothly with the number A of nucleons, and a shell correction contribution obtained from a suitable single-particle potential for the fine tuning.

The macroscopic-microscopic calculations predict spherical shell closures at $Z = 114$ and $N = 184$ [9]. Self-consistent Hartree-Fock calculations with a variety of Skyrme forces show the most pronounced shell effects at $Z = 124, 126$ and $N = 184$ [10–13]. As an exception to this rule, Skyrme parametrizations such as SkI3 and SkI4 which have a modified spin-orbit interaction prefer $Z = 120$ and $Z = 114$, respectively, for the proton shell closure [11,12]. Hartree-Fock-Bogoliubov calculations with the finite range Gogny force predict $Z = 120, 126$

and $N = 172, 184$ as possible shell closures [11,12]. The relativistic mean field (RMF) theory with the conventional scalar and vector meson field couplings typically prefers $Z = 120$ and $N = 172$ as the best candidates for spherical shell closures [10–13]. Of course, the different nature of the spin-orbit interaction in the Skyrme and RMF models is pivotal in deciding the location of the stronger shell effects. Detailed comparisons between Skyrme Hartree-Fock and RMF calculations of SHE can be found in Refs. [11] and [13].

The discrepancies in the predicted shell closures motivate us to reinvestigate them using the more general RMF model derived from the chiral effective Lagrangian proposed by Furnstahl, Serot and Tang [15–17]. This model is a new approach to the nuclear many-body problem which combines the modern concepts of effective field theory (EFT) and density functional theory (DFT) for hadrons.

An EFT assumes that there exist natural scales to a given problem and that the only degrees of freedom relevant for its description are those which can unravel the dynamics at the scale concerned. The unresolved dynamics corresponding to heavier degrees of freedom is encoded in the coupling constants of the theory, which are determined by fitting them to known experimental data. The Lagrangian of Furnstahl, Serot and Tang is intended as an EFT of low-energy QCD. As such, its main ingredients are the lowest-lying hadronic degrees of freedom and it has to incorporate all the infinite (in general non-renormalizable) couplings consistent with the underlying symmetries of QCD. To endow the model with predictive power the Lagrangian is expanded and truncated. Terms that contribute at the same level are grouped together with the guidance of naive dimensional analysis [18]. Truncation at a certain order of accuracy is consistent only if the coupling constants eventually exhibit naturalness (i.e., if they are of order unity when in appropriate dimensionless form). In the nuclear structure problem the basic expansion parameters are the ratios of the scalar and vector meson fields and of the Fermi momentum to the nucleon mass M , as these ratios are small in normal situations. To solve the equations of motion that stem from the constructed effective Lagrangian one applies the relativistic mean field approximation in which the meson fields are replaced by their classical expectation values.

EFT and DFT are bridged by interpreting the expansion of the effective Lagrangian as equivalent to an expansion of the energy functional of the many-nucleon system in terms of nucleon densities and auxiliary meson fields. The RMF theory is then viewed as a covariant formulation of DFT in the sense of Kohn and Sham [19]. That is, the mean field model approximates the exact, unknown energy functional of the ground-state densities of the nucleonic system, which includes all higher-order correlations, using powers of auxiliary classical meson fields. This merger of EFT and DFT provides an approach to the nuclear problem which retains the simplicity of solving variational Hartree equations with the bonus that further contributions, at the mean field level or beyond, can be incorporated in a systematic and controlled manner.

If the chiral effective Lagrangian is truncated at fourth order, in mean field approach one recovers the same couplings of the usual non-linear $\sigma - \omega$ model plus additional non-linear scalar-vector and vector-vector meson interactions, besides tensor couplings [16,17]. The free parameters of the resulting energy functional have been fitted to ground-state observables of a few doubly-magic nuclei. The fits, parameter sets named G1 and G2 [16], do display naturalness and are not dominated by the last terms retained; an evidence which confirms the usefulness of the EFT concepts and validates the truncation of the effective Lagrangian at the first lower orders. The ideas of EFT have been fruitful [20], moreover, to elucidate the empirical success of previous RMF models, like the original $\sigma - \omega$ model of Walecka [21] and its non-linear extensions with cubic and quartic scalar self-interactions [22]. However, these conventional RMF models truncate the effective Lagrangian at some level without further physical rationale or symmetry arguments. The introduction of new interaction terms in the effective model pursues an improved representation of the relativistic energy functional [16,17].

In a previous work we have studied the impact of the new couplings of the EFT model on the properties of nuclear matter and of the nuclear surface [23]. In Ref. [24] we have shown that the EFT model provides a unified framework to accommodate the successful phenomenology of the traditional RMF models for finite nuclei, and to extend them reliably

for applications in regions of densities moderately higher than at saturation where the mean field approximation is still suitable. In Ref. [25] we tested the ability of the EFT model for describing ground-state properties of different isotopic (isotonic) chains with a magic number of protons (neutrons), from the valley of β stability up to the drip lines. For the calculation of open-shell nuclei we employed a modified BCS approach, with a constant pairing strength, which takes into account quasibound levels owing to their centrifugal barrier. It turned out that the G1 and G2 sets plus this residual pairing interaction describe the experimental systematics of one- and two-nucleon separation energies and of rms radii, from the proton to the neutron drip line, with a similar quality to standard RMF force parameters like NL-SH or NL3 [26–28]. Very recently, the convergence of the EFT approach has been studied for some specific doubly-magic nuclei far from stability [29] and remarkable agreement with experiment has been found.

With the above positive experience at hand, and as a next step of our program, in the present paper we want to investigate the predictability of the new effective Lagrangian approach to the nuclear many-body problem in extrapolations to superheavy and hyperheavy nuclei. We shall focus on analyzing the model predictions for spherical shell closures. Though deformation is an important degree of freedom for SHE [30–32], we are searching for spherical shell stability around $Z = 114 - 120$ and $N = 172 - 184$ where deformation is known to be small [30], and in hyperheavy nuclei around $N \sim 258$ which is also believed to be spherical [33]. Therefore, our calculations will be restricted to spherical symmetry. Deformation would change the picture in details and add deformed shell closures, e.g., like those predicted around $Z = 108$ and $N = 162$ [31], but it would not change the predictions for the spherical shell effect. Our analysis uses the EFT parameter sets G1 and G2 [16], with the above-mentioned prescription for pairing. The results will be compared with those obtained with the NL3 parameter set [34], taken as one of the best representatives of the usual RMF model with only scalar self-interactions.

The paper is organized as follows. In the second section we first briefly summarize the RMF model derived from EFT and we next describe our modified BCS approach to pairing.

The third section is devoted to the study of several properties of superheavy nuclei such as two-particle separation energies and shell gaps, average pairing gaps, single-particle energy spectra, and shell corrections. We also discuss some relevant features of the particle densities and spin-orbit potentials. We compare the results obtained from the EFT parametrizations G1 and G2 with the corresponding results of the NL3 set. The summary and conclusions are laid in the fourth section.

II. FORMALISM

A. The model

The EFT model used here has been developed in Ref. [16]. Further insight into the model and the concepts underlying it can be gained from Refs. [15,17,20,35]. For our purposes, the basic ingredient is the EFT energy density functional for finite nuclei. It reads [16,17]

$$\begin{aligned}
\mathcal{E}(\mathbf{r}) = & \sum_{\alpha} \varphi_{\alpha}^{\dagger} \left\{ -i\boldsymbol{\alpha} \cdot \boldsymbol{\nabla} + \beta(M - \Phi) + W + \frac{1}{2}\tau_3 R + \frac{1 + \tau_3}{2} A \right. \\
& - \frac{i}{2M} \beta \boldsymbol{\alpha} \cdot \left(f_v \boldsymbol{\nabla} W + \frac{1}{2} f_{\rho} \tau_3 \boldsymbol{\nabla} R + \lambda \boldsymbol{\nabla} A \right) + \frac{1}{2M^2} (\beta_s + \beta_v \tau_3) \Delta A \left. \right\} \varphi_{\alpha} \\
& + \left(\frac{1}{2} + \frac{\kappa_3}{3!} \frac{\Phi}{M} + \frac{\kappa_4}{4!} \frac{\Phi^2}{M^2} \right) \frac{m_s^2}{g_s^2} \Phi^2 - \frac{\zeta_0}{4!} \frac{1}{g_v^2} W^4 \\
& + \frac{1}{2g_s^2} \left(1 + \alpha_1 \frac{\Phi}{M} \right) (\boldsymbol{\nabla} \Phi)^2 - \frac{1}{2g_v^2} \left(1 + \alpha_2 \frac{\Phi}{M} \right) (\boldsymbol{\nabla} W)^2 \\
& - \frac{1}{2} \left(1 + \eta_1 \frac{\Phi}{M} + \frac{\eta_2}{2} \frac{\Phi^2}{M^2} \right) \frac{m_v^2}{g_v^2} W^2 - \frac{1}{2g_{\rho}^2} (\boldsymbol{\nabla} R)^2 - \frac{1}{2} \left(1 + \eta_{\rho} \frac{\Phi}{M} \right) \frac{m_{\rho}^2}{g_{\rho}^2} R^2 \\
& - \frac{1}{2e^2} (\boldsymbol{\nabla} A)^2 + \frac{1}{3g_{\gamma} g_v} A \Delta W + \frac{1}{g_{\gamma} g_{\rho}} A \Delta R. \tag{1}
\end{aligned}$$

The coupling constants have been written so that in the present form they should be of order unity according to the naturalness assumption. The index α runs over all occupied nucleon states $\varphi_{\alpha}(\mathbf{r})$ of the positive energy spectrum. The meson fields are $\Phi \equiv g_s \phi_0(\mathbf{r})$, $W \equiv g_v V_0(\mathbf{r})$ and $R \equiv g_{\rho} b_0(\mathbf{r})$, and the photon field is $A \equiv e A_0(\mathbf{r})$. Variation of the energy

density (1) with respect to φ_α^\dagger and the meson fields gives the Dirac equation fulfilled by the nucleons and the Klein-Gordon equations obeyed by the mesons (see Refs. [16,23] for the detailed expressions). We solve the Dirac equation in coordinate space by transforming it into a Schrödinger-like equation. The set of coupled equations is iterated numerically till consistency is reached.

As we have mentioned in the Introduction, the energy density (1) can be interpreted in the context of a density functional theory formulation [16,17,36], with the local meson fields playing the role of Kohn-Sham potentials. The exact energy density functional of the nuclear many-body system would consist of kinetic, Hartree and exchange-correlation parts. In the RMF approach one approximates the exact functional by an expansion in powers of the classical meson fields and their derivatives. If the parameters of the expansion are fitted to experimental data, the functional will automatically incorporate the effects of many-body corrections beyond the Hartree level. That is, a mean field Dirac-Hartree calculation can be viewed as being equivalent to a density functional approach, in which higher-order many-body effects are treated approximately.

For the sake of completeness we next summarize some of the implications of the new terms of the energy density (1). The quartic vector self-interaction ζ_0 and the terms η_1 and η_2 make it possible to obtain a desirable positive value of the coupling constant κ_4 of the quartic scalar self-interaction, for realistic nuclear matter properties and keeping all the parameters within the bounds of naturalness. These bulk couplings confer an extra density dependence to the scalar and vector self-energies which is consistent with the output of microscopic Dirac-Brueckner-Hartree-Fock calculations [24]. In the standard RMF model the only parameter not related with the saturation conditions is the mass of the scalar meson m_s . The additional couplings α_1 and α_2 are helpful to improve on the description of the nuclear surface properties (e.g., surface energy and surface thickness) without spoiling the bulk properties [23]. In the EFT model the bulk symmetry energy coefficient J depends on the coupling η_ρ in addition to the usual coupling g_ρ . The new coefficient η_ρ is useful to fit J and in turn to tune, relative to J , the stiffness of the nucleus against pulling neutrons

apart from protons as the neutron excess is increased [23]. The quantities β_s , β_v , g_γ and $\lambda = \frac{1}{2}\lambda_p(1 + \tau_3) + \frac{1}{2}\lambda_n(1 - \tau_3)$ take care of effects related with the electromagnetic structure of the pion and the nucleon ($g_\gamma^2/4\pi = 2.0$, $\lambda_p = 1.793$ and $\lambda_n = -1.913$ are given their experimental values) [16]. More important in the context of SHE may be the role of the tensor coupling f_v between the ω meson and the nucleon. It introduces a corrective term in the spin-orbit potential as compared with the expression in the standard RMF model [25,37]. This term may have some impact on the splitting of large angular momentum states which often determine the shell closures in the SHE [11,13].

In this work we shall employ the EFT parameter sets G1 and G2 of Ref. [16]. The masses of the nucleon and of the ω and ρ mesons are $M = 939$ MeV, $m_\omega = 782$ MeV and $m_\rho = 770$ MeV, respectively. The parameters m_s , g_s , g_v , g_ρ , η_1 , η_2 , η_ρ , κ_3 , κ_4 , ζ_0 , f_v , α_1 , and α_2 of G1 and G2 were fitted by a least-squares optimization procedure to 29 observables (binding energies, charge form factors and spin-orbit splittings near the Fermi surface) of the nuclei ^{16}O , ^{40}Ca , ^{48}Ca , ^{88}Sr and ^{208}Pb , as described in Ref. [16]. The constants β_s , β_v and f_ρ were then chosen to reproduce the experimental charge radii of the nucleon. We report in Table 1 the values of the parameters and the saturation properties of the sets G1 and G2 as well as those of the NL3 parametrization [34]. A satisfactory feature of the set G2 is that it presents a positive value of κ_4 , as opposite to G1 and to most of the successful RMF parametrizations such as NL3. We note that the value of the effective mass at saturation M_∞^*/M in the EFT sets (~ 0.65) is somewhat larger than the usual value in the RMF parameter sets (~ 0.60), which is due to the presence of the tensor coupling f_v of the ω meson to the nucleon [25,37].

B. Pairing

In order to describe open-shell nuclei the pairing correlations have to be explicitly taken into account. The most popular approach for well-bound isotopes has been the BCS method. However, the BCS approximation breaks down for exotic nuclei near the drip lines because it does not treat the coupling to the continuum properly. This difficulty is disposed of either

by the non-relativistic Hartree-Fock-Bogoliubov theory, with Skyrme [38] and Gogny [39] forces, or by the relativistic Hartree-Bogoliubov (RHB) theory. The RHB approach relies on the relativistic model for the mean field part and the D1S Gogny force, or some variant, for the pairing channel [26–28,40,41]. Recent calculations with Skyrme forces together with a zero-range interaction in the pairing channel have shown that a corrected BCS approach, which includes some quasibound states due to their centrifugal barrier, is able to provide a good qualitative estimate of the pairing effects close to the drip lines [42]. These quasibound states mock up the influence of the continuum in the pairing calculation.

Pairing correlations are another important ingredient in the study of superheavy elements. Furthermore, some of the predicted regions of shell stability in superheavy nuclei lie close to the drip point and a suitable treatment is required. Many calculations of SHE have often used a zero-range two-body pairing force $V_{pair} = V_{0,p/n}\delta(\mathbf{r} - \mathbf{r}')$, with adjustable strengths for protons and neutrons (see Refs. [11,13]). A study of SHE using the RHB approach, with the NL-SH parameter set, was carried out in Ref. [43].

To deal with the pairing correlations we use here a simplified prescription which we have found to be in acceptable agreement with RHB calculations [25]. For each kind of nucleon we assume a constant pairing matrix element G_q , which simulates the zero range of the pairing force, and include quasibound levels in the BCS calculation as done in Ref. [42]. These levels of positive single-particle energy are retained by the centrifugal barrier (neutrons) or the centrifugal-plus-Coulomb barrier (protons). The wave functions of the considered quasibound levels are mainly localized in the classically allowed region and decrease exponentially outside it. As a consequence, the unphysical nucleon gas which surrounds the nucleus if continuum levels are included in the normal BCS approach is eliminated. We have shown in Ref. [25], by comparison with available RHB results, that our procedure is able to predict well the position of the proton and neutron drip lines or, e.g., the behavior of the neutron and charge radii far from stability. Also, the calculated pairing gaps turn out to be scattered around the empirical average $12/\sqrt{A}$ MeV.

In our treatment the pairing equations reduce to [44]

$$\frac{G_q}{2} \sum_{\alpha_q > 0} \frac{1}{\sqrt{(\varepsilon_{\alpha_q} - \mu_q)^2 + \Delta_q^2}} = 1, \quad (2)$$

$$\frac{1}{2} \sum_{\alpha_q > 0} \left[1 - \frac{\varepsilon_{\alpha_q} - \mu_q}{\sqrt{(\varepsilon_{\alpha_q} - \mu_q)^2 + \Delta_q^2}} \right] = A_q, \quad (3)$$

where the subindex q stands for each kind of nucleon, $\alpha_q = \{nljm\}_q$ is the set of quantum numbers which identify each state, and A_q is the number of neutrons or protons involved in the pairing correlation. We restrict the available space of α_q states to one harmonic oscillator shell above and below of the Fermi level, to avoid the unrealistic pairing of highly excited states and to confine the region of influence of the pairing potential to the vicinity of the Fermi level. The solution of Eqs. (2) and (3) allows one to find the chemical potential μ_q and the average gap Δ_q for each kind of nucleon. The pairing energy reads

$$E_{\text{pair}} = - \sum_q \frac{\Delta_q^2}{G_q}. \quad (4)$$

We write the pairing matrix elements as $G_q = C_q/A$, where the C_q are constants. We have fixed the C_q coefficients by looking for the best agreement of our calculation with the known experimental binding energies of Ni and Sn isotopes for neutrons, and of $N = 28$ and $N = 82$ isotones for protons [25]. The values obtained from these fits are $C_n = 21$ MeV and $C_p = 22.5$ MeV for the G1 set, $C_n = 19$ MeV and $C_p = 21$ MeV for the G2 set, and $C_n = 20.5$ MeV and $C_p = 23$ MeV for the NL3 interaction.

In Ref. [25] we already applied this improved BCS approach with the G1 and G2 parametrizations to study one- and two-neutron (proton) separation energies for several chains of isotopes (isotones) from stability to the drip lines. We found a reasonable agreement with the available experimental data, similar to the one obtained using the NL3 set. Apart from shifts of one or two units of A , the position of the neutron and proton drip lines was reached at the same place with the G1, G2 and NL3 sets. The analysis showed that the parameters sets based on EFT are able to describe nuclei far from the β -stability valley when a pairing residual interaction is included. Notice that only information about a few stable magic nuclei was used in the fit of the coupling constants of the G1 and G2 sets, and

thus the results near the drip lines are predictions of the EFT model.

III. RESULTS AND DISCUSSION

Traditionally a large gap in the single-particle spectrum has been interpreted as an indicator of a shell closure, at least for nuclei of atomic number $Z < 100$. However, for a large nucleus like a superheavy element, it may not be sufficient to simply draw the single-particle level scheme and to look for the gaps, due to the complicated structure of the spectrum and the presence of levels with a high degree of degeneracy. Moreover, in a self-consistent calculation, a strong coupling between the neutron and proton shell structure takes place. Therefore, when dealing with SHE it is imperative to look for other quantities to reliably identify the shell closures and magic numbers, apart from the analysis of the single-particle level structure.

Here we shall consider the following observables as indicators for shell closures:

a) A sudden jump in the two-neutron (two-proton) separation energies of even-even nuclei, defined as

$$S_{2q} = E(N_q - 2) - E(N_q), \quad (5)$$

where N_q is the number of neutrons (protons) in the nucleus for $q = n$ ($q = p$). A sharp drop in S_{2q} means that a very small amount of energy is required to remove two more nucleons from the remnant of the parent nucleus. Thus, the parent nucleus is more stable which is a character of magicity. This observable is an efficient tool to quantify the shell effect because of the absence of odd-even effects [11].

b) The size of the gap in the neutron (proton) spectrum is determined by half of the difference in Fermi energy when going from a closed shell nucleus to a nucleus with two additional neutrons (protons). This quantity is very well accounted for by the two-neutron (two-proton) shell gap which is defined as the second difference of the binding energy [10,11]:

$$\delta_{2q}(N_q) = S_{2q}(N_q) - S_{2q}(N_q + 2) = E(N_q + 2) - 2E(N_q) + E(N_q - 2). \quad (6)$$

This quantity measures the size of the step found in the two-nucleon separation energy and, therefore, it is strongly peaked at the magic numbers.

c) The neutron and proton average pairing gaps Δ_q of open-shell nuclei can be related to the odd-even mass difference, from where the empirical law $\Delta \sim 12/\sqrt{A}$ can be derived [44]. However, for closed shell nuclei Δ_q should vanish. Thus, we shall use the vanishing of the average pairing gap [obtained from Eqs. (2) and (3)] as another signal for identifying closed shell nuclei.

We next calculate the above observables for the isotopic chain of $Z = 120$ and for several isotonic chains, assuming spherical symmetry. We employ the parameter sets G1 and G2 due to the EFT formalism and compare the results with those obtained from the standard RMF parametrization NL3, which is well established as a successful interaction for nuclei at and away from the line of β stability.

It is to be mentioned that the previous indicators correspond to energy differences between neighbouring nuclei. However, they do not have a direct connection with the shell corrections which stabilize a given (N, Z) superheavy nucleus against fission [13]. The shell corrections are related to the difference between the nuclear binding energies and the predictions of a liquid-drop model. As a complementary study, after our search for spherical shell closures, we shall analyze the shell corrections for the discussed chains of SHE.

A. Isotopic chain of $Z = 120$

We first consider the chain of isotopes with atomic number $Z = 120$, which is found as a magic number in recent relativistic mean field calculations of nuclei in the superheavy mass region [10–13]. Figure 1 collects the results obtained with the EFT parameter set G2. The two-neutron separation energies S_{2n} are displayed in the upper panel of this figure. The S_{2n} graph shows a smooth decrease with increasing neutron number N throughout the whole chain except for the sudden jumps after the neutron numbers $N = 172, 184,$ and 258 . These jumps indicate the possible occurrence of a shell closure at these neutron numbers. Using

Eq. (6) we calculate the two-nucleon shell gap for neutrons for the same isotopic chain, and present the result in the middle panel of Figure 1. Sharp peaks in δ_{2n} are found at the same neutron numbers 172, 184, and 258. It is seen that the peaks of $N = 172$ and $N = 258$ are more marked than the peak of $N = 184$. Actually, the height of the peak at $N = 184$ is around only one third of that of the peak at $N = 172$. One may note that the amplitude of the jumps in δ_{2n} for shell closures is smaller in the SHE region than in the region of normal mass nuclei. This is expected due to the increase of the single-particle level density with increasing mass number. For example, for ^{208}Pb and for the doubly-magic isotopes of tin and calcium we find values of δ_{2n} between some 5 and 10 MeV.

The average pairing gap Δ_q is representative of the strength of the pairing correlations. The curve for the neutron pairing gaps, displayed in the bottom panel of Figure 1, shows a structure of arches that vanish only at $N = 172, 184, \text{ and } 258$. Since the proton pairing gap Δ_p is zero throughout the whole chain, we have not plotted it. Although we use a simplified prescription for the calculation of the pairing gap, which is provided by the solution of Eqs. (2) and (3), our value for Δ_q can be considered as an average of the different state-dependent single-particle gaps which would be obtained if one had used a zero-range pairing force, as done e.g. in Refs. [11,13].

Therefore, all of the three analyzed observables are pointing to the same neutron numbers as the best candidates for shell closures for $Z = 120$ with the G2 parametrization. It is to be kept in mind that only for doubly-magic nuclei one can guarantee a spherical shape. For open-shell nuclei the spherical solution does not always correspond to the ground state. Inclusion of deformation would likely yield some extra stability for $Z = 120$ nuclei other than $^{292}120$, $^{304}120$ and $^{378}120$. Nevertheless, the spherical solution gives a firsthand and overall view of the sequence of spherical shell closures.

In order to analyze the force dependence of the location of the shell closures for the superheavy nuclei, we calculate the quantities S_{2n} , δ_{2n} and Δ_n with the EFT set G1 and with the NL3 parameter set for the same isotopic chain $Z = 120$ and display the results in Figures 2 and 3, respectively. As in the case of the G2 set, the proton pairing gap Δ_p

vanishes for the whole chain of $Z = 120$ isotopes and it is not drawn. The global nature of the curves of Figures 2 and 3 is quite similar to that observed previously with the G2 set. Abrupt jumps in S_{2n} and δ_{2n} , and the vanishing of the average neutron pairing gap Δ_n , indicate shell closures at $N = 172$ and 258 in both of the G1 and NL3 sets. The height of the peaks of δ_{2n} at $N = 172$ and 258 is very similar between the G1 and G2 sets, while they attain the largest values in the NL3 set. For the $N = 184$ system, S_{2n} and δ_{2n} show only a moderate jump in both G1 and NL3, indicating a weaker shell closure than for $N = 172$ and 258 . Moreover, the neutron pairing gap Δ_n does not vanish at $N = 184$ with the G1 and NL3 sets, contrarily to the case of G2.

One expects a relatively large energy gap to appear between the last occupied and the first unoccupied single-particle levels for the neutron numbers corresponding to the shell closures detected above. Let us now look into the neutron single-particle spectra, displayed in Figure 4, for the $^{292}120$, $^{304}120$ and $^{378}120$ nuclei. All the three parameter sets G2, G1 and NL3 show a large gap above the Fermi energy for $N = 172$ and 258 . But for the neutron number $N = 184$, there appear only moderate gaps across the Fermi level for the G2 and G1 sets, and the gap is still smaller for NL3. This is in agreement with our previous discussions of the other indicators.

Inspecting the $N = 258$ level spectrum one can appreciate another visible energy gap across the neutron numbers $N = 228$ ($1k_{17/2}$ level) and $N = 198$ ($1j_{13/2}$ level) in all of the parameter sets. In spite of this, no distinct indications for a shell closure were found for $N = 228$ or $N = 198$ in the curves of S_{2n} , δ_{2n} , and Δ_n in Figures 1–3. If one compares the spectra for the three systems $N = 172$, 184 , and 258 , it can be noticed that the gap between two particular levels is strongly modified along the isotopic chain. Consequently, an analysis of the spectra alone would not suffice and the use of the discussed energy indicators becomes mandatory in order to make predictions for shell closures in superheavy nuclei.

The occupancy of the single-particle levels, which is closely related with the pairing gap, can also provide an indication for the closed shell nuclei. We compare in Figure 5 the occupancies of the single-particle levels lying around the Fermi level for $N = 182$, 184 , and

186 obtained from the G2 and NL3 parameter sets (with $Z = 120$). From Figure 5 one can see that for the G2 set the occupancy goes from 1 to 0 just after the Fermi level for $N = 184$, which we found as a magic number in our calculation. But for the other open-shell nuclei $N = 182$ and 186 a tail is found in the occupancy curve beyond the Fermi energy. For the NL3 parameter set we find the tail structure in the occupancy even for $N = 184$, which indicates that particles are diffused beyond the Fermi level. Thus, we can say that $N = 184$ is not a shell closure in the NL3 parameter set.

B. Isotonic chains

We now proceed to discuss the isotonic chains of the neutron numbers which we have detected as candidates for spherical shell closures in the preceding study of the isotopic chain of $Z = 120$. We start with the $N = 172$ isotonic chain in Figure 6, which displays the two-proton separation energy S_{2p} , the two-proton shell gap δ_{2p} , and the average pairing gaps Δ_p and Δ_n in the superheavy region from $Z = 100$ up to the proton drip line, for the EFT model G2 and for the conventional RMF model NL3. For brevity we do not present the results from the G1 set, since the previous section has shown that the predictions of G2 differ from NL3 more than in the case of G1.

From Figure 6 one realizes that all the indicators signal a very robust shell closure at $Z = 120$, and a much weaker shell closure at $Z = 114$. The proton gap δ_{2p} (~ 5 MeV) of the nucleus $^{292}120$ is nearly twice as large as the corresponding neutron gap δ_{2n} (~ 3 MeV, Figures 1 and 3). For the NL3 set, in addition, a little jump in S_{2p} and a small peaked structure in δ_{2p} indicates the possibility of a weak shell closure taking place at $Z = 106$. It is nevertheless known that the region around $Z = 106$ is deformed [33] and thus the spherical solution does not correspond to the ground state. Moreover, from the bottom panel of Figure 6, we see that the neutron pairing gap Δ_n vanishes from $Z = 110$ till the proton drip point, but it is non-zero for smaller atomic numbers. The non-vanishing neutron pairing gap for the ($N = 172, Z = 106$) combination tells us that this cannot be a doubly-closed

shell nucleus. Therefore, the neutron number $N = 172$ exhibits a strong shell closure for the proton number $Z = 120$ but this magicity is washed out for $Z \leq 110$. In conclusion, in the region of superheavy nuclei the magicity of a particular neutron number depends on the number of protons present in the nucleus.

We next analyze the shell closures for $N = 184$ and $N = 258$ in combination with different proton numbers. In Figure 7 we display the results for the $N = 184$ isotonic chain. Curves are somewhat similar to those for $N = 172$. In the G2 parametrization one identifies $Z = 114$ and $Z = 120$ as possible shell closures though the size of the jump in δ_{2p} , which is similar for both proton numbers, is small if we compare it with the jump observed for ($N = 172, Z = 120$) in Figure 6. In the case of the NL3 parameter set there is some evidence for a weak shell closure at $Z = 114$ only, because the neutron pairing gap for $Z = 120$ does not vanish which prevents the combination ($N = 184, Z = 120$) from representing a doubly-magic nucleus. The results for $N = 258$ neutrons are shown in Figure 8. We again find a strong signature for a shell closure at $Z = 120$ in both the G2 and NL3 parameter sets, whereas the indications for a shell closure at $Z = 114$ are much weaker. One also observes prominent jumps in S_{2p} and δ_{2p} at $Z = 132$ (NL3) and $Z = 138$ (NL3 and G2). But in this region, close to the proton drip line, the neutron pairing gap does not vanish. This implies that only the combination of $N = 258$ with proton numbers $Z = 114$ and $Z = 120$ may exhibit a double shell closure character.

Figure 9 depicts the proton single-particle spectra obtained with the G2 and NL3 parametrizations for the illustrative examples of the $^{286}_{114}$, $^{292}_{120}$, $^{298}_{114}$, and $^{304}_{120}$ nuclei. Looking at the proton spectra for the systems with $N = 172$, a very large gap can be observed for 120 protons (between the $2f_{5/2}$ and $3p_{3/2}$ levels for G2, and between the $2f_{5/2}$ and $1i_{11/2}$ levels for NL3). Instead, practically no gap exists for 114 protons (between the $2f_{7/2}$ and $2f_{5/2}$ levels), specially for the NL3 set. This is consistent with the very weak signals of magicity of $Z = 114$ in the case of the $N = 172$ isotonic chain shown by the S_{2p} and δ_{2p} indicators in Figure 6.

With the addition of only 12 neutrons, the proton spectra for the systems with $N = 184$

exhibit a different pattern than for $N = 172$ near the Fermi energy (cf. Figure 9). The gaps occurring between the levels corresponding to 114 protons and to 120 protons are now comparable in magnitude. This fact is in agreement with the relatively magic character of the $^{298}114$ and $^{304}120$ nuclei predicted by the indicators plotted in Figure 7. In any case, even for $N = 184$, the magicity of $Z = 114$ is always smaller than the one shown by $Z = 120$, as one can see from the comparison of S_{2p} and δ_{2p} in Figures 6 and 7. This discussion shows again the strong dependence of the proton (neutron) shell closures of SHE on the neutron (proton) numbers and thus the importance of using the energy indicators.

C. Shell corrections

The stability of superheavy elements with an atomic number larger than $Z \sim 100$ is possible thanks to the shell effects. In the liquid droplet model picture these superheavy nuclei are unstable against spontaneous fission because the large Coulomb repulsion can no longer be compensated by the nuclear surface tension. However, SHE may still exist because the quantal shell corrections generate local minima in the nuclear potential energy surface which provide additional stabilization.

In our context the shell correction energy is also useful as a different test for checking the robustness of the shell closures. For experimentally known shell closures, i.e., up to $Z = 82$ and $N = 126$, the shell corrections are strongly peaked around the magic numbers (see, e.g., Refs. [46,47]), providing enhanced binding for magic nuclei. However, in the superheavy mass region, instead of displaying sharp jumps, the shell corrections depict a landscape of rather broad areas of shell stabilized nuclei [12,33]. Still, in these areas the closed shell nuclei show a larger stabilization (i.e., more negative shell corrections) than their neighbours. In the present subsection we want to study the shell corrections around our selected nuclei with $Z = 114$ and $Z = 120$, and $N = 172$, 184, and 258.

The calculation of the shell correction energy is based on the Strutinsky energy theorem [45] which states that the total quantal energy can be divided in two parts:

$$E = \tilde{E} + E_{\text{shell}}. \quad (7)$$

The largest piece \tilde{E} is the average part of the energy which depends in a smooth way on the number of nucleons (namely, the part well represented by the liquid droplet model). The smaller piece, the shell correction E_{shell} , has instead an oscillating behaviour. The oscillations are due to the grouping of levels into shells and display maxima at the shell closures.

According to the idea of Strutinsky, the average part of the ground-state energy of a shell model potential can be obtained by replacing the Hartree-Fock occupation numbers n_α (1 or 0 for occupied or empty states) with occupation numbers \tilde{n}_α smoothed by some averaging function. The shell correction E_{shell} is computed as the difference of the exact energy to that average part (for brevity we do not separate the neutron and proton parts in the following expressions):

$$E_{\text{shell}} = \sum_{\alpha} (n_{\alpha} - \tilde{n}_{\alpha}) \varepsilon_{\alpha}, \quad (8)$$

with ε_{α} being the energy eigenvalues of the nuclear potential. The smoothed \tilde{n}_{α} are subject to the normalization condition and are written in terms of an average level density $\tilde{g}(\varepsilon)$:

$$N = \sum_{\alpha} \tilde{n}_{\alpha} = \int_{-\infty}^{\tilde{\mu}} d\varepsilon \tilde{g}(\varepsilon), \quad (9)$$

which also fixes the value of the smooth chemical potential $\tilde{\mu}$. The average level density $\tilde{g}(\varepsilon)$ is obtained by folding the quantal level density $g(\varepsilon) = \sum_{\alpha} \delta(\varepsilon - \varepsilon_{\alpha})$ with a smoothing function $f(x)$ taken over a certain energy range γ of the order of the separation between shells ($\gamma \sim \hbar\omega$):

$$\tilde{g}(\varepsilon) = \frac{1}{\gamma} \int_{-\infty}^{\infty} d\varepsilon' g(\varepsilon') f\left(\frac{\varepsilon - \varepsilon'}{\gamma}\right) = \frac{1}{\gamma} \sum_{\alpha} f\left(\frac{\varepsilon - \varepsilon_{\alpha}}{\gamma}\right), \quad (10)$$

where $f(x)$ is constructed as the product of a Gaussian by an even polynomial of degree $2M$ (curvature correction) [44]. For Eq. (8) to hold, the averaged energy must be independent of γ (plateau condition).

The Strutinsky smoothing procedure requires the use of several major shells, and this faces the problem of the treatment of the continuum when realistic finite depth potentials are employed. One possibility is to resort to the states resulting from the diagonalization of the self-consistent potential in a large harmonic oscillator basis [48]. However, many unphysical states with positive energy appear in this approach and it is not well suited for weakly bound nuclei [49]. To overcome this deficiency, a Green's function procedure has been applied for the calculation of the shell correction in superheavy nuclei [12,33]. In the present work we follow a different strategy, consistently with our approach to the treatment of pairing. Working in coordinate space, we perform the Strutinsky smoothing including the quasibound levels which are retained by their centrifugal barrier (centrifugal-plus-Coulomb barrier for protons). We have taken 7 major shells above the Fermi energy (i.e., states up to around 50 MeV above the Fermi level) and have considered curvature corrections up to $2M = 10$. We have found that the plateau condition is fulfilled for a smoothing parameter $\gamma \sim 1.3 - 1.6$ MeV for both protons and neutrons. As we have discussed, the quasibound levels included in our calculation do not depend on the size of the box where the calculation is performed. These levels, usually with high angular momentum, lie close in energy to the RHB canonical levels [25]. Of course, one limitation of our approach is that some resonant levels with low angular momentum can be missed, more easily for neutrons, and then their contribution is shared among the higher angular momentum levels which we include in the calculation.

The total (neutron-plus-proton) shell corrections stemming from our calculations for the isotopic chains with $Z = 114$ and $Z = 120$ are displayed in Figure 10. The equivalent graph for the isotonic chains with $N = 172, 184,$ and 258 is presented in Figure 11. Again, we point out that our calculation is performed in spherical symmetry and thus the calculated shell corrections represent in general an upper bound to the actual ones. Stronger shell stabilization could still be provided by deformation. The magnitude of the shell correction energy E_{shell} is dictated by the level density around the Fermi level. A high level density in the vicinity of the Fermi energy yields a positive shell correction reducing the binding

energy, whereas a low level density gives a negative shell correction which increases the binding energy. The shell corrections obtained with the G2 and NL3 sets are rather similar for the investigated isotopic and isotonic chains. This is so because the single-particle levels around the Fermi surface essentially show the same ordering with both parameter sets and there are only small differences in the spin-orbit splittings, as it can be realized from Figures 4 and 9. The results for the set G1 are also similar to those of G2 and NL3 and thus we do not display them in Figures 10 and 11.

In Figure 10 the isotopic chain of $Z = 120$ shows a large negative shell correction at $N = 172$, due to the presence of low angular momentum levels near the Fermi energy for both neutrons ($4s_{1/2}$, $3d_{3/2}$ and $3d_{5/2}$ levels) and protons ($3p_{1/2}$ and $3p_{3/2}$ levels). These levels imply a comparatively lower level density and thus a more negative shell correction. The isotopic chain also shows another local minimum around $N = 182 - 184$, but in this case the shell correction energy is less negative than for $N = 172$. The pattern exhibited by the total shell correction for the $Z = 120$ isotopes looks very similar to that of the neutron shell correction displayed in Figure 5 of Ref. [12] for the NL3 parameter set, which was computed by means of the Green's function procedure. Looking at the curves for the $Z = 114$ isotopic chain represented in Figure 10 one realizes that the shell corrections are globally weaker than that for $Z = 120$ chain, which means less stability. They also present minima at $N = 172$ and at $N = 184$, although in this case the situation is reversed and the largest corrections correspond to $N = 184$ instead of $N = 172$.

In the upper panel of Figure 11 the shell corrections for the $N = 172$ isotonic chain clearly show only one minimum at $Z = 120$. The $N = 184$ chain (middle panel) displays one more local minimum at $Z = 114$, though the magnitude of the shell correction obtained for $Z = 114$ is smaller than for $Z = 120$. Our total shell corrections for $N = 172$ and $N = 184$ show similar patterns to the proton shell corrections of NL3 which are depicted in Figure 6 of Ref. [12] for these same isotonic chains. The curves of the shell correction for the $N = 258$ hyperheavy nuclei (lower panel of Figure 11) are overall very much flat in comparison to those for the isotonic chains of $N = 172$ and $N = 184$. The absolute minimum again appears

at $Z = 120$. There is also a very small kink at $Z = 114$. The comparison of the curves in the 3 panels reveals that at $Z = 120$ all the curves show the most prominent minima. At $Z = 114$, the shell corrections for $N = 172$ have no dip at all, but they display a small kink for $N = 184$ and $N = 258$.

From the analysis of the shell correction energy we see that the location of the minima in the shell stabilized regions of SHE is in good agreement with the conclusions about the shell closures that we inferred from the study of the previous indicators. Due to the fact that the minima in the shell corrections for superheavy nuclei are often not very pronounced, but rather shallow, we note the usefulness of analyzing the shell corrections as a complementary means to assess the predictions made on the basis of the energy indicators.

D. Density profiles and spin-orbit potentials

From a naive point of view one expects that for a large nucleus the neutron density profile will show a relatively flat region at the interior, modulated by some wiggles due to shell effects. In the case of protons one also expects that the Coulomb repulsion will push them towards the surface so that the proton density will develop a depression in the center. However, some deviations from this pattern can arise in superheavy nuclei. To exemplify the situation, we display in Figure 12 the density profiles of neutrons and protons for the superheavy nuclides $^{292}120$ (close to the proton drip point), $^{304}120$, and $^{378}120$ (close to the neutron drip point). For the purpose of comparison with the situation in smaller nuclei, we have drawn in the same figure the neutron and proton density profiles of the isotopes ^{100}Sn (proton drip line nucleus), ^{132}Sn , and ^{176}Sn (neutron drip line nucleus).

Inspecting the behavior of the tin isotopes with increasing neutron number N , one observes that the neutron density extends progressively toward the outside, while it shows only a small increase in the interior. Driven by the proton-neutron interaction, the proton density also extends more and more to the outside. As a result, since $Z = 50$ is fixed, there is a notable reduction of the average proton density in the nuclear interior. (See Ref. [27]

for a detailed RHB study of the tin chain.) These general trends are also observed in the evolution with N of the nucleon densities of the $Z = 120$ isotopes displayed on the left side of Figure 12.

It is immediately noted that the neutron density profile of the $^{292}120$ superheavy nucleus shows an accentuated dip from $r \sim 4$ fm to the origin. As also pointed out in Ref. [11], the reason lies in the fact that for $N = 172$ the last filled neutron levels correspond to a large orbital angular momentum (2g and 1j levels, see Figure 4). Such orbits are mainly located at the surface and thus generate the central dip. This is not the case for the system with $N = 184$, where the last occupied neutron levels (4s and 3d) give an important contribution to the central density. For $N = 258$ neutrons the situation lies somehow in between of the two previous cases due to the contribution of the 4p and 3f orbitals near the Fermi level. For the tin isotopes shown in Figure 12, the neutron orbits in the vicinity of the Fermi energy consist of a bunch of low angular momentum levels together with the intruder level of higher angular momentum. The neutron density profiles of the three tin isotopes show the normal pattern, though for $N = 50$ one can recognize a dip around the center which has the same nature discussed for the superheavy nucleus $N = 172$, now because of the 1g neutron level.

The proton density profiles of the three superheavy isotopes of $Z = 120$ depicted in Figure 12 show a similar pattern. Again, there is an effect due to the orbitals around the Fermi level. The 2f and 1i proton orbits of the $Z = 120$ nuclides (see Figure 9) push their protons away from the center and as a consequence the proton density develops a pocket around $r \sim 2$ fm. On the other hand, the increase of the proton density which is observed close to the origin is reminiscent of the fingerprint of the 3s protons. The proton densities of the tin isotopes also exhibit a depression near the center. This time it is occasioned by the 1g proton level, which is the last filled level for $Z = 50$. However, due to the smaller Coulomb repulsion and to the 2p orbits close in energy to the 1g level, the effect is not as remarkable as for the proton density of $Z = 120$.

We now come to the discussion of the spin-orbit potential in the superheavy mass region, because it is responsible for the strong reduction of the spin-orbit splitting of low angular

momentum energy levels which is usually found in self-consistent calculations of SHE. In the relativistic models the spin-orbit force is automatically included in the interaction from the outset. It appears explicitly when the lower spinor of the relativistic wave function is eliminated in favor of the upper spinor. One then obtains a Schrödinger-like equation that contains a spin-orbit term which reads [37,41]:

$$H_{so} = \frac{1}{2\bar{M}^2} V_{so}(r) \mathbf{L} \cdot \mathbf{S}, \quad (11)$$

$$V_{so}(r) = \frac{M^2}{\bar{M}^2} \frac{1}{r} \left(\frac{d\Phi}{dr} + \frac{dW}{dr} \right) + 2f_v \frac{M}{\bar{M}} \frac{1}{r} \frac{dW}{dr}, \quad (12)$$

where we have made $\bar{M} = M - \frac{1}{2}(\Phi + W)$. This spin-orbit potential includes the contribution of the tensor coupling of the ω meson to the nucleon, which has an important bearing on the spin-orbit force [16,23,37]. For simplicity, we have neglected in (12) the small contributions of the ρ meson and of the Coulomb field which make $V_{so}(r)$ slightly different for neutrons and protons.

Figure 13 displays the radial dependence of V_{so} given by Eq. (12) for the isotopes of $Z = 120$ and $Z = 50$, whose density distributions we have just discussed. A common feature of both the tin and the superheavy isotopes is that, as expected, the spin-orbit potential develops a well at the surface region of the nuclear density distributions. As the system becomes more and more neutron rich, the depth of this well experiments a gradual reduction and the position of the bottom of the potential is shifted outwards, which brings about a weaker spin-orbit force.

There are two distinctive trends of the spin-orbit potential of superheavy nuclei with respect to normal nuclei. One is that the spin-orbit well at the surface is less deep in the case of the SHE. The other one is the strong upward bump that V_{so} develops around 2 – 4 fm from the origin. This bump can be explained in connection with the spatial distribution of the densities. Consider the case of $N = 172$. The nucleon densities are sharply reduced in the center (Figure 12). To the extent that the meson fields follow the change of the densities, this causes V_{so} to develop a sharp bump in the interior of the nucleus [11,13]. As seen from

Figure 13, the ensuing bump is largest for $N = 172$ and decreases with increasing neutron number as the central region of the neutron densities flattens out.

The strong increase of V_{so} near the origin has an outstanding effect on the energy splitting of spin-orbit partner levels in SHE. Large angular momentum states whose wave function is mostly localized around the nuclear surface basically feel the attractive part of V_{so} , and thus present normal spin-orbit splittings. However, for low angular momentum states there is a strong overlap of the wave function with the positive region of V_{so} which dramatically reduces the spin-orbit splittings (they may even have the opposite sign for some parameter sets [11]). This effect is corroborated by looking at the splittings of spin-orbit partners in the SHE spectra represented in Figures 4 and 9.

Little differences are seen in Figure 13 between the predictions of the G2 and NL3 sets for the spin-orbit potential. The higher effective mass at saturation of G2 ($M_\infty^* = 0.66$) with respect to NL3 ($M_\infty^* = 0.6$) is compensated by the contribution of the tensor coupling f_v in the G2 set, since there exists a trade-off between the size of the ω tensor coupling and the size of the scalar field [23,37]. As noticed in Ref. [25] the contribution of f_v to Eq. (12) accounts for roughly one-third of the spin-orbit strength in the case of the G2 parameter set.

Still, inspecting Figure 13, one may observe that the bottom of V_{so} is located at slightly larger values of r in the G2 set than in the NL3 set. Also, the spin-orbit well at the surface tends to be slightly deeper in G2 than in NL3 for the $Z = 120$ isotopes (the opposite happens for tin between $N = 50$ and $N = 82$). Finally, the upward bumps appearing in the spin-orbit potential of the SHE at $r \sim 3$ fm are larger if V_{so} is calculated with NL3. Thus, it may be expected that the spin-orbit splitting of low angular momentum energy levels of SHE will be smaller with NL3 than with G2. Since for the SHE the strength of V_{so} at the surface is a little stronger and shifted towards slightly larger distances, the spin-orbit splitting for high angular momentum energy levels should be larger with G2 than with NL3. These predictions for the splittings of the energy levels of SHE coming from the small differences in V_{so} obtained with the two considered parameter sets, can be seen in the proton and

neutron single-particle spectra displayed in Figures 4 and 9.

IV. SUMMARY AND CONCLUSIONS

We have analyzed the properties of superheavy nuclei searching for spherical shell closures beyond $Z = 82$ and $N = 126$. We have carried out the study using the G1 and G2 parametrizations of Ref. [16] obtained from the modern effective field theory approach to relativistic nuclear phenomenology. We have compared the results with those computed with the NL3 parameter set which is one of the most successful conventional RMF models.

To detect the shell closures in SHE we have considered several energy indicators. Namely, within an isotopic or isotonic chain of SHE the shell closures are identified by a simultaneous occurrence at a given Z or N of a large jump in the corresponding two-nucleon separation energy S_{2q} , a pronounced peak in the two-nucleon shell gap δ_{2q} , and the vanishing of the average pairing gaps Δ_n and Δ_p . To treat the pairing correlations we have employed an improved BCS model that was used successfully in Ref. [25] in calculations of isotopic and isotonic chains with magic proton or neutron numbers.

First we have studied the isotopic chain of $Z = 120$, which is found to be a magic number in previous RMF calculations. Neutron shell closures arise at $N = 172$ and $N = 258$ in all the considered parameter sets (G1, G2 and NL3). In the particular case of the G2 set $N = 184$ appears as another possible neutron shell closure, though it is not as robust as for $N = 172$ or $N = 258$. The magic character of $Z = 120$ is supported by the fact that the average proton pairing gap vanishes along the whole isotopic chain. Next we have investigated the isotonic chains with $N = 172, 184$ and 258 for $Z > 100$. From this analysis the candidates to proton shell closures have been found to be $Z = 114$ (weakly) and $Z = 120$ (strongly). Other possible candidates different from $Z = 114$ and $Z = 120$ present a non-vanishing neutron pairing gap.

We conclude that the parameter sets G1 and G2 derived from the effective field theory approach clearly point out towards the doubly-magic character of the ($N = 172, Z = 120$)

and $(N = 258, Z = 120)$ combinations, which is in agreement with the predictions of the NL3 set. The magicity of the neutron numbers $N = 172$ and $N = 258$ for $Z = 120$ protons can also be noticed in the neutron single-particle spectra of these isotopes, which show a considerably large energy gap at the indicated neutron numbers. One can also recognize a moderate neutron shell gap occurring at $N = 184$, which is a little larger in G1 and G2 than in NL3. The study of the proton single-particle spectra of the $N = 172$ isotones clearly reveals a proton shell closure at $Z = 120$, whereas $Z = 114$ does not present evidences of magicity. However, if one considers the isotones of $N = 184$ the proton energy gaps which appear in the proton spectra at $Z = 114$ and $Z = 120$ are comparable in magnitude (although definitely smaller than the energy gap at $Z = 120$ when $N = 172$). Thus, a particular proton shell closure can be modified depending on the number of neutrons present in the nucleus, and viceversa, due to the tight coupling between the neutron and proton shell structures in the self-consistent calculation of SHE. This means that it is not possible anymore to calculate the spectra of one (N, Z) combination as a representative for a whole region of superheavy nuclei.

A minimum condition for a superheavy nucleus to be stable against fission is that the shell effects must be able to provide enough binding to compensate for the huge Coulomb repulsion among protons. Compared to normal nuclei where the large negative shell corrections are peaked at the magic numbers, the SHE display broad areas of shell stabilization around the possible shell closures. We have computed the shell corrections for the analyzed superheavy nuclei by means of an Strutinsky smoothing. The continuum has been parametrized by taking quasibound levels which in coordinate space are retained by their centrifugal barrier.

We have found a region of shell stabilization for the isotopes of $Z = 114$ and $Z = 120$ in the range of neutron numbers $N \sim 170 - 186$. The shell corrections are larger for $Z = 120$ than for $Z = 114$, and in both cases show peaks at $N = 172$ and $N = 184$ which indicates the larger stability of these nuclei relative to their neighbours. For the isotonic chains of $N = 172$ and $N = 184$ the more negative shell corrections appear at $Z = 120$, although a smaller peak shows up at $Z = 114$ pointing out the relatively stable character of this nucleus,

at least compared with the immediate neighbours. The curve of the shell corrections for the isotones of $N = 258$ is mostly flat, but again a depression can be recognized around $Z = 120$. From the analysis of the shell corrections it turns out that the more stable superheavy nuclei correspond well with the candidates to exhibiting a double shell closure detected in the study of the energy indicators.

The nuclear density distributions of SHE predicted by the EFT parameter sets and by NL3 display similar trends. In particular, for the isotopes of $Z = 120$ they all show a depression near the center of the proton density profile. It is originated from the high orbital angular momentum of the proton energy levels that lie below the Fermi energy for $Z = 120$. These levels are mainly located around the surface, which adds to the effect of the Coulomb repulsion in the center of the nucleus. A similar situation occurs in the neutron density of the $N = 172$ system, where only high angular momentum states are involved below the Fermi energy. In a self-consistent calculation the trends of the nuclear density are followed by the spatial distribution of the spin-orbit potential, which in turn determines the splitting of the energy levels. Thus, as a consequence of the effect discussed for the density profiles, the spin-orbit potentials of SHE show a prominent bump near the center, in addition to the usual spin-orbit well located at the nuclear surface. This pattern strongly reduces the spin-orbit splitting of low orbital angular momentum levels, while levels with a large orbital angular momentum present normal splittings.

To summarize, in previous works [24,25] we showed that the parameter sets derived from the effective field theory approach to the low-energy nuclear many-body problem [16] work nicely for both β -stable and β -unstable nuclei. This is in addition to their ability to yield a realistic equation of state at densities above saturation [24]. In the present study we have applied the EFT model to deal with the theoretical description of some properties of superheavy nuclei. In particular, we have seen that the G1 and G2 parameter sets reproduce the strong double shell closure at $N = 172$ and $Z = 120$ predicted by the standard RMF parametrizations. The EFT sets also predict a double shell closure at $N = 258$ and $Z = 120$, in agreement with the results obtained with the NL3 set and with the doubly magic character

of this nucleus pointed out in earlier literature. Interestingly enough, the new parameter set G2 shows some evidence for a double shell closure of the $N = 184$, $Z = 114$ nucleus traditionally predicted by the macroscopic-microscopic models, as well as by the Skyrme interaction SkI4.

ACKNOWLEDGMENTS

Two of us (X. V. and M. C.) acknowledge financial support from the DGI (Ministerio de Ciencia y Tecnología, Spain) and FEDER under grant BFM2002-01868 and from DGR (Catalonia) under grant 2001SGR-00064. T. S. thanks the Spanish Education Ministry grant SB2000-0411 for financial support and the Departament d'Estructura i Constituents de la Matèria of the University of Barcelona for kind hospitality.

REFERENCES

- [1] S. Hofmann, Rep. Prog. Phys. **61**, 639 (1998); Eur. Phys. J. **A15**, 195 (2002).
- [2] S. Hofmann, and G. Münzenberg, Rev. Mod. Phys. **72**, 733 (2000).
- [3] P. Armbruster, Ann. Rev. Nucl. Part. Sci. **50**, 411 (2000).
- [4] Yu. Ts. Oganessian *et al*, Eur. Phys. J. **A5**, 63 (1999); Nature **400**, 242 (1999); Eur. Phys. J. **A15**, 201 (2002).
- [5] W. D. Myers, and W. J. Swiatecki, Nucl. Phys. **A81**, 1 (1966).
- [6] A. Sobiczewski, F. A. Gareev, and B. N. Kalinkin, Phys. Lett. **22**, 500 (1966).
- [7] S. G. Nilsson *et al.*, Nucl. Phys. **A115**, 545 (1968).
- [8] U. Mosel and W. Greiner, Z. Phys. **222**, 261 (1969).
- [9] P. Möller, and J. R. Nix, Nucl. Phys. **A549**, 84 (1992); J. Phys. **G20**, 1681 (1994).
- [10] K. Rutz, M. Bender, T. Bürvenich, T. Schilling, P.-G. Reinhard, J.A. Maruhn, and W. Greiner, Phys. Rev. **C56**, 238 (1997).
- [11] M. Bender, K. Rutz, P.-G. Reinhard, J.A. Maruhn, and W. Greiner, Phys. Rev. **C60**, 034304 (1999).
- [12] A. T. Kruppa, M. Bender, W. Nazarewicz, P.-G. Reinhard, T. Vertse, and S. Ówiok, Phys. Rev. **C61**, 034313 (2000).
- [13] P. -G. Reinhard, M. Bender, and J.A. Maruhn, Comm. Mod. Phys. **2**, A177 (2002).
- [14] J. -F. Berger, L. Bitaud, J. Dechargé, M. Girodi, and K. Dietrich, Nucl. Phys. **A685**, 1 (2001).
- [15] R. J. Furnstahl, B. D. Serot, and H. B. Tang, Nucl. Phys. **A598**, 539 (1996).
- [16] R. J. Furnstahl, B. D. Serot, and H. B. Tang, Nucl. Phys. **A615**, 441 (1997); *ibid.*

- A640**, 505 (1998).
- [17] B. D. Serot, and J. D. Walecka, Int. J. Mod. Phys. **E6**, 515 (1997).
- [18] H. Georgi, Phys. Lett. **B298**, 187 (1993).
- [19] W. Kohn, and L. J. Sham, Phys. Rev. A **140**, 1133 (1965).
- [20] R. J. Furnstahl, and B. D. Serot, Nucl. Phys. **A671**, 447 (2000).
- [21] B. D. Serot, and J. D. Walecka, Adv. Nucl. Phys. **16**, 1 (1986).
- [22] J. Boguta, and A. R. Bodmer, Nucl. Phys. **A292**, 413 (1977).
- [23] M. Del Estal, M. Centelles, and X. Viñas Nucl. Phys. **A650**, 443 (1999).
- [24] M. Del Estal, M. Centelles, X. Viñas, and S. K. Patra, Phys. Rev. **C63**, 024314 (2001);
M. Centelles, M. Del Estal, X. Viñas, and S. K. Patra, *The Nuclear Many-Body Problem 2001*, NATO Science Series II Vol. 53 (Kluwer, Dordrecht, 2002), p. 97.
- [25] M. Del Estal, M. Centelles, X. Viñas, and S. K. Patra, Phys. Rev. **C63**, 044321 (2001).
- [26] J. Meng, Phys. Rev. **C57**, 1229 (1998); Nucl. Phys. **A635**, 3 (1998).
- [27] J. Meng and I. Tanihata, Nucl. Phys. **A650**, 176 (1999).
- [28] D. Vretenar, G. A. Lalazissis and P. Ring, Phys. Rev. **C57**, 3071 (1998).
- [29] M. A. Huertas, Phys. Rev. **C66**, 024318 (2002).
- [30] R. Smolańczuk, Phys. Rev. **C56**, 812 (1997).
- [31] T. Bürvenich, K. Rutz, M. Bender, P.-G. Reinhard, J. A. Maruhn, and W. Greiner,
Eur. Phys. J. **A3**, 139 (1998).
- [32] S.K. Patra, W. Greiner, and R.K. Gupta, J. Phys **G26**, L65 (2000).
- [33] M. Bender, W. Nazarewicz, P.-G. Reinhard, Phys. Lett. **B515**, 42 (2001).

- [34] G.A. Lalazissis, J. König and P. Ring, Phys. Rev. **C55**, 540 (1997).
- [35] J. J. Rusnak and R. J. Furnstahl, Nucl. Phys. **A627**, 495 (1997).
- [36] C. Speicher, R. M. Dreizler and E. Engel, Ann. Phys. (NY) **213**, 312 (1992).
- [37] R. J. Furnstahl, J. J. Rusnak and B. D. Serot, Nucl. Phys. **A632**, 607 (1998).
- [38] J. Dobaczewski, H. Flocard, and J. Treiner, Nucl. Phys. **A422**, 103 (1984); J. Dobaczewski, W. Nazarewicz, T. R. Werner, J.-F. Berger, R. C. Chin, and J. Dechargé, Phys. Rev. C **53**, 2809 (1996).
- [39] J. Dechargé, and D. Gogny, Phys. Rev. **C21**, 1568 (1980).
- [40] T. Gonzalez-Llarena, J. L. Egido, G. A. Lalazissis, and P. Ring, Phys. Lett. **B379**, 13 (1996).
- [41] G.A. Lalazissis, D. Vretenar and P. Ring, Phys. Rev. **C57**, 2294 (1998).
- [42] E. Chabanat, P. Bonche, P. Haensel, J. Meyer, and R. Schaeffer, Nucl. Phys. **A635**, 231 (1998).
- [43] G.A. Lalazissis, M. M. Sharma, P. Ring, and Y. K. Gambhir, Nucl. Phys. **A608**, 202 (1996).
- [44] P. Ring and P. Schuck, *The Nuclear Many-Body Problem* (Springer-Verlag, Berlin, 1980).
- [45] V. M. Strutinsky, Nucl. Phys. **A122**, 1 (1968); Nucl. Phys. **A218**, 169 (1974).
- [46] M. Kleban, B. Nerlo-Pomorska, J. F. Berger, J. Dechargé, M. Girod, and S. Hilaire, Phys. Rev. **C65**, 024309 (2002).
- [47] B. Nerlo-Pomorska, K. Pomorski, J. Bartel, and K. Dietrich, Phys. Rev. **C66**, 051302 (2002).
- [48] M. Bolsterli, E. O. Fiset, J. R. Nix, and J. L. Norton, Phys. Rev. C **5**, 1050 (1972).

- [49] W. Nazarewicz, T. R. Werner, and J. Dobaczewski, *Phys. Rev. C* **50**, 2860 (1994); T. Vertse, A. T. Kruppa, R. J. Liotta, W. Nazarewicz, N. Sandulescu, and T. R. Werner, *Phys. Rev. C* **57**, 3089 (1998).

TABLES

TABLE I. Parameters of the relativistic interactions used in this work, in dimensionless form, and their saturation properties in nuclear matter (energy per particle, density, incompressibility, effective mass, and symmetry energy coefficient).

	G1	G2	NL3
m_s/M	0.540	0.554	0.541
$g_s/4\pi$	0.785	0.835	0.813
$g_v/4\pi$	0.965	1.016	1.024
$g_\rho/4\pi$	0.698	0.755	0.712
κ_3	2.207	3.247	1.465
κ_4	-10.090	0.632	-5.668
ζ_0	3.525	2.642	0.0
η_1	0.071	0.650	0.0
η_2	-0.962	0.110	0.0
η_ρ	-0.272	0.390	0.0
α_1	1.855	1.723	0.0
α_2	1.788	-1.580	0.0
$f_v/4$	0.108	0.173	0.0
$f_\rho/4$	1.039	0.962	0.0
β_s	0.028	-0.093	0.0
β_v	-0.250	-0.460	0.0
a_v (MeV)	-16.14	-16.07	-16.24
ρ_∞ (fm ⁻³)	0.153	0.153	0.148
K (MeV)	215.0	215.0	271.5
M_∞^*/M	0.634	0.664	0.595
J (MeV)	38.5	36.4	37.40

FIGURE CAPTIONS

Figure 1. The change with the neutron number N of the two-neutron separation energy S_{2n} , the two-neutron shell gap δ_{2n} , and the neutron average pairing gap Δ_n for $Z = 120$ isotopes obtained from spherical calculations with the relativistic parameter set G2. The proton average pairing gap Δ_p vanishes in the whole isotopic chain.

Figure 2. Same as Figure 1 but for the relativistic parameter set G1.

Figure 3. Same as Figure 1 but for the relativistic parameter set NL3.

Figure 4. Single-particle spectrum of neutrons in the vicinity of the Fermi level for the superheavy isotopes $^{292}120$, $^{304}120$, and $^{378}120$ computed with the relativistic interactions G1, G2 and NL3.

Figure 5. Occupancy of the neutron single-particle levels located around the Fermi energy for the $Z = 120$ isotopes with $N = 182$, 184, and 186 obtained from the G2 and NL3 parameter sets.

Figure 6. The change with the proton number Z of the two-proton separation energy S_{2p} , the two-proton shell gap δ_{2p} , and the proton Δ_p and neutron Δ_n average pairing gaps for $N = 172$ isotones obtained from spherical calculations with the relativistic parameter sets G2 (left panels) and NL3 (right panels).

Figure 7. Same as Figure 6 but for the isotones of $N = 184$.

Figure 8. Same as Figure 6 but for the isotones of $N = 258$.

Figure 9. Single-particle spectrum of protons in the vicinity of the Fermi level for the superheavy isotones $^{286}114$ and $^{292}120$ (left panel), and $^{298}114$ and $^{304}120$ (right panel) computed with the relativistic interactions G2 and NL3.

Figure 10. The change of the total shell correction energy (sum of the neutron and proton contributions) with the neutron number N for the isotopes of $Z = 114$ and $Z = 120$ in

spherical calculations with the G2 and NL3 models.

Figure 11. The change of the total shell correction energy (sum of the neutron and proton contributions) with the proton number Z for the isotonic chains of $N = 172$, $N = 184$, and $N = 258$ neutrons in spherical calculations with the G2 and NL3 models.

Figure 12. The radial neutron and proton density distributions predicted by the sets G2 and NL3 for the $Z = 120$ superheavy isotopes with $N = 172$, 184, and 258 (left panels), in comparison with the results for the tin isotopes with $N = 50$, 82, and 126 (right panels).

Figure 13. Same as Figure 12 but for the radial dependence of the spin-orbit potential V_{so} defined in Eq. (12).

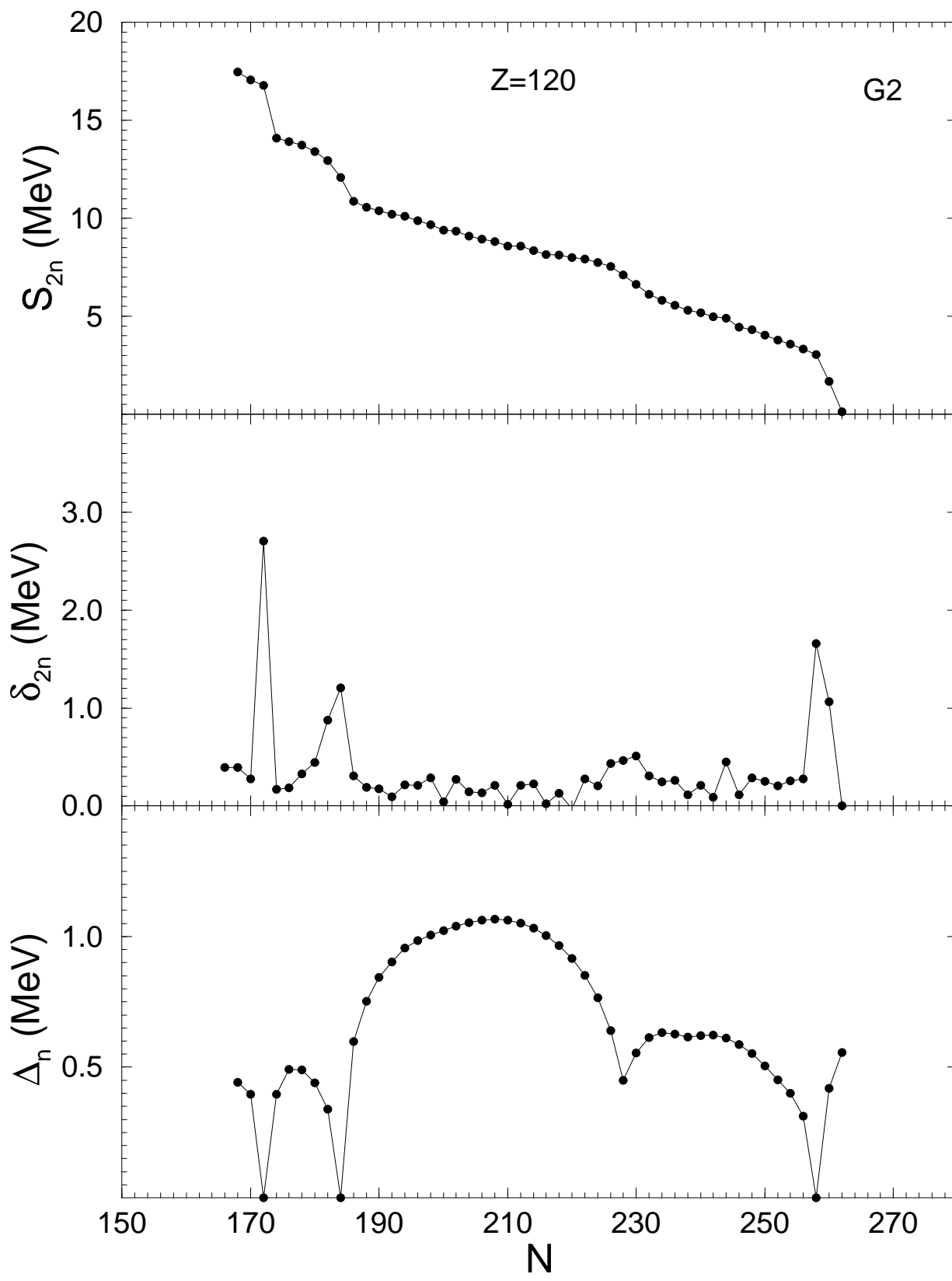


Fig. 1

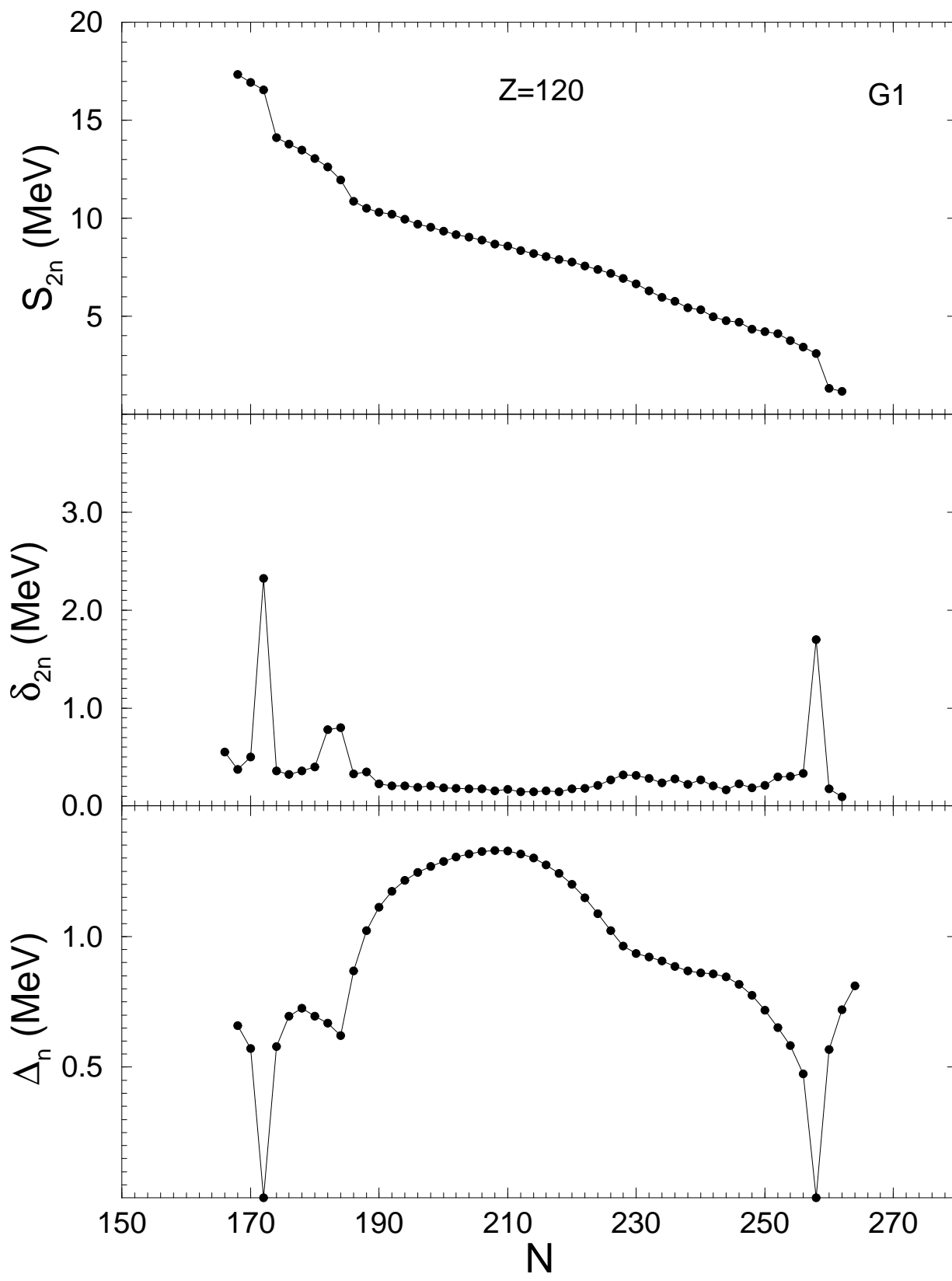


Fig. 2

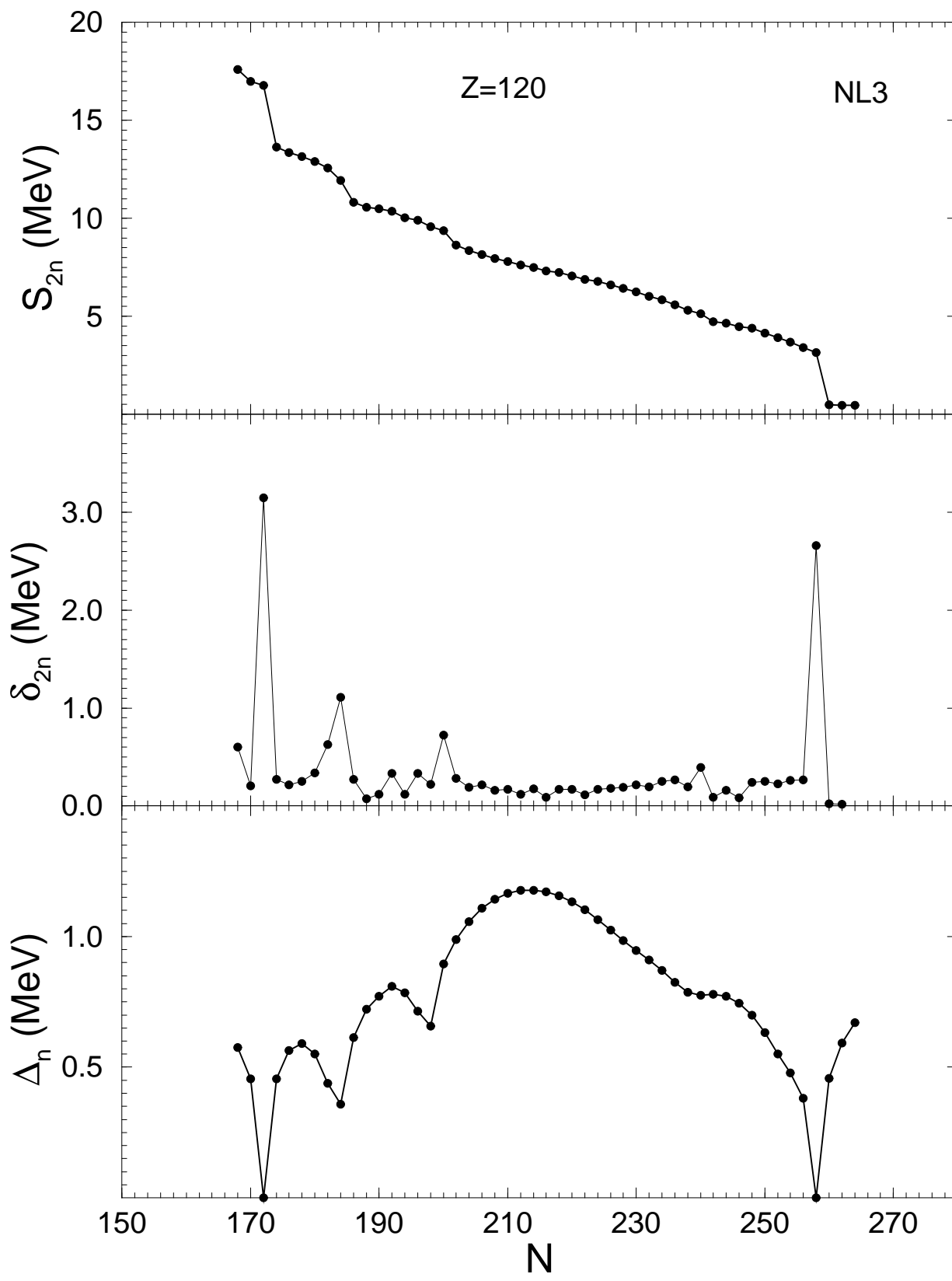


Fig. 3

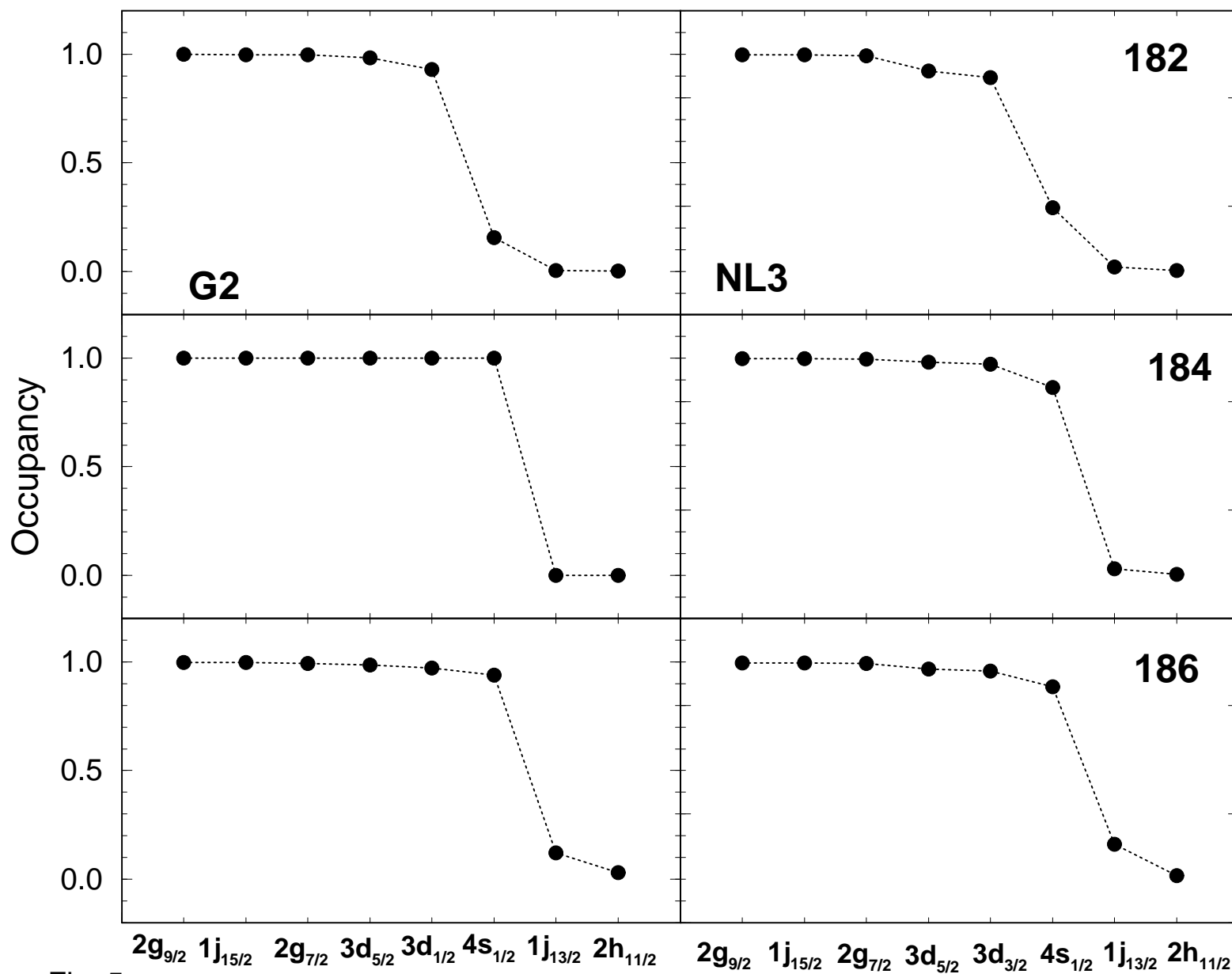


Fig. 5

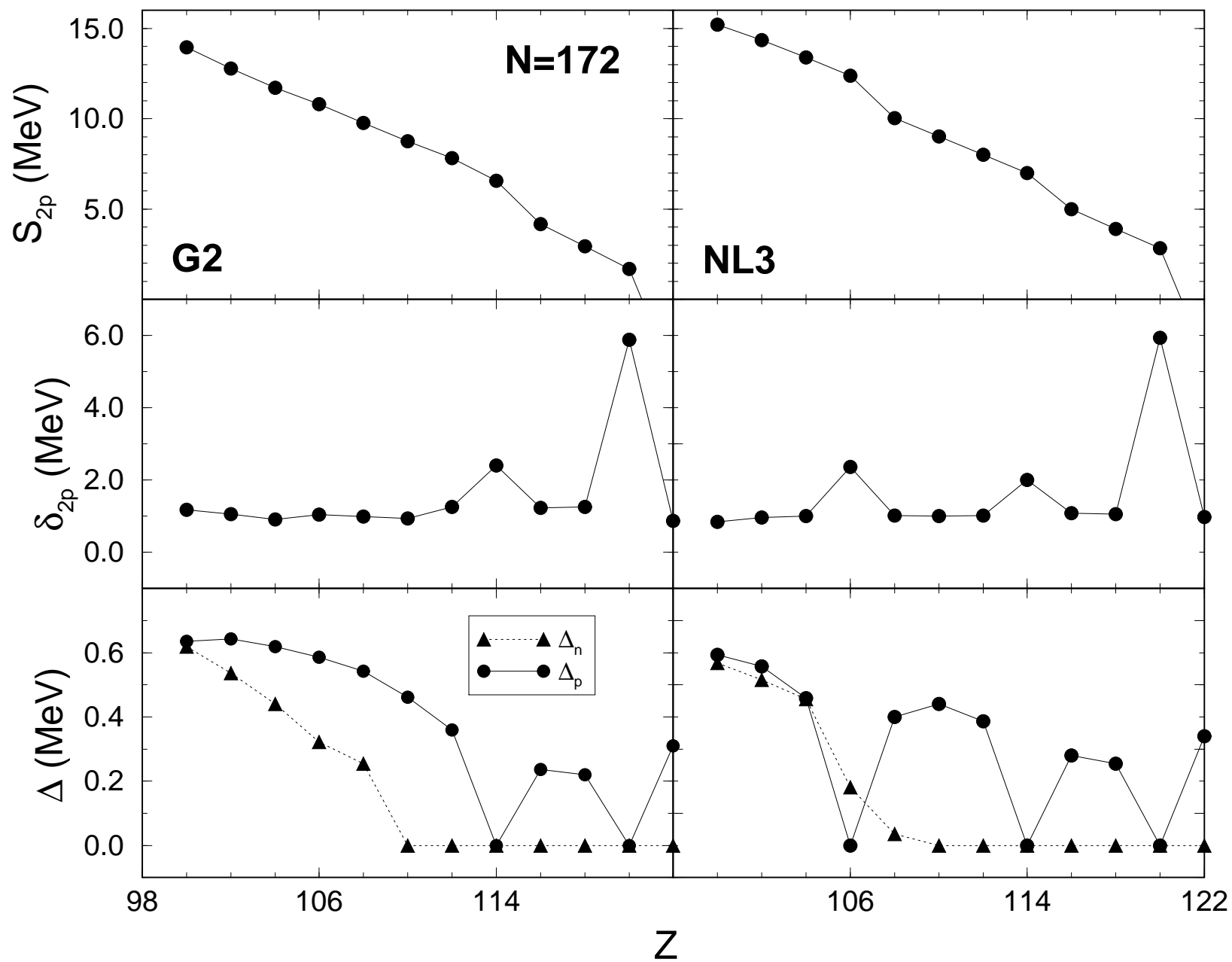


Fig. 6

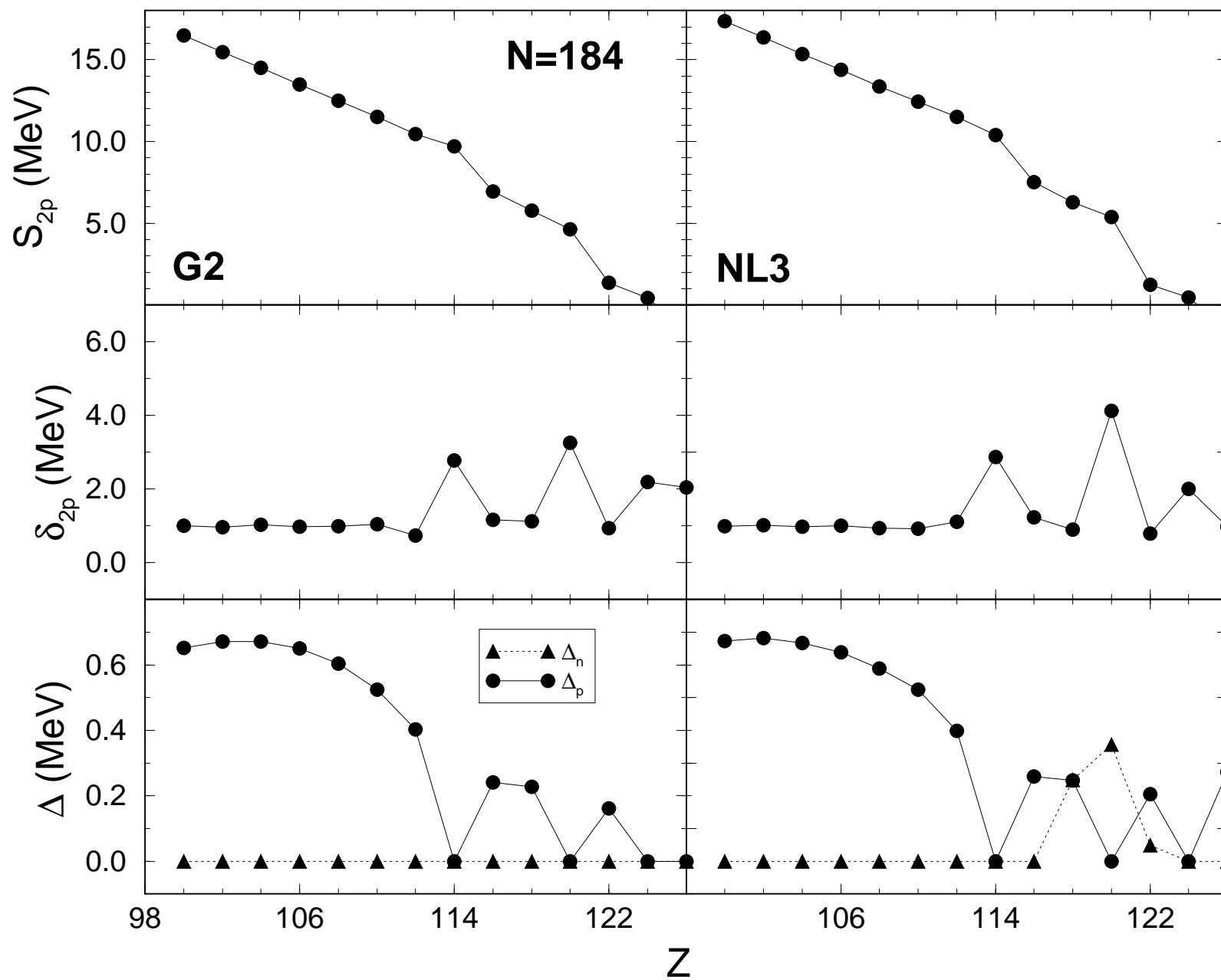


Fig. 7

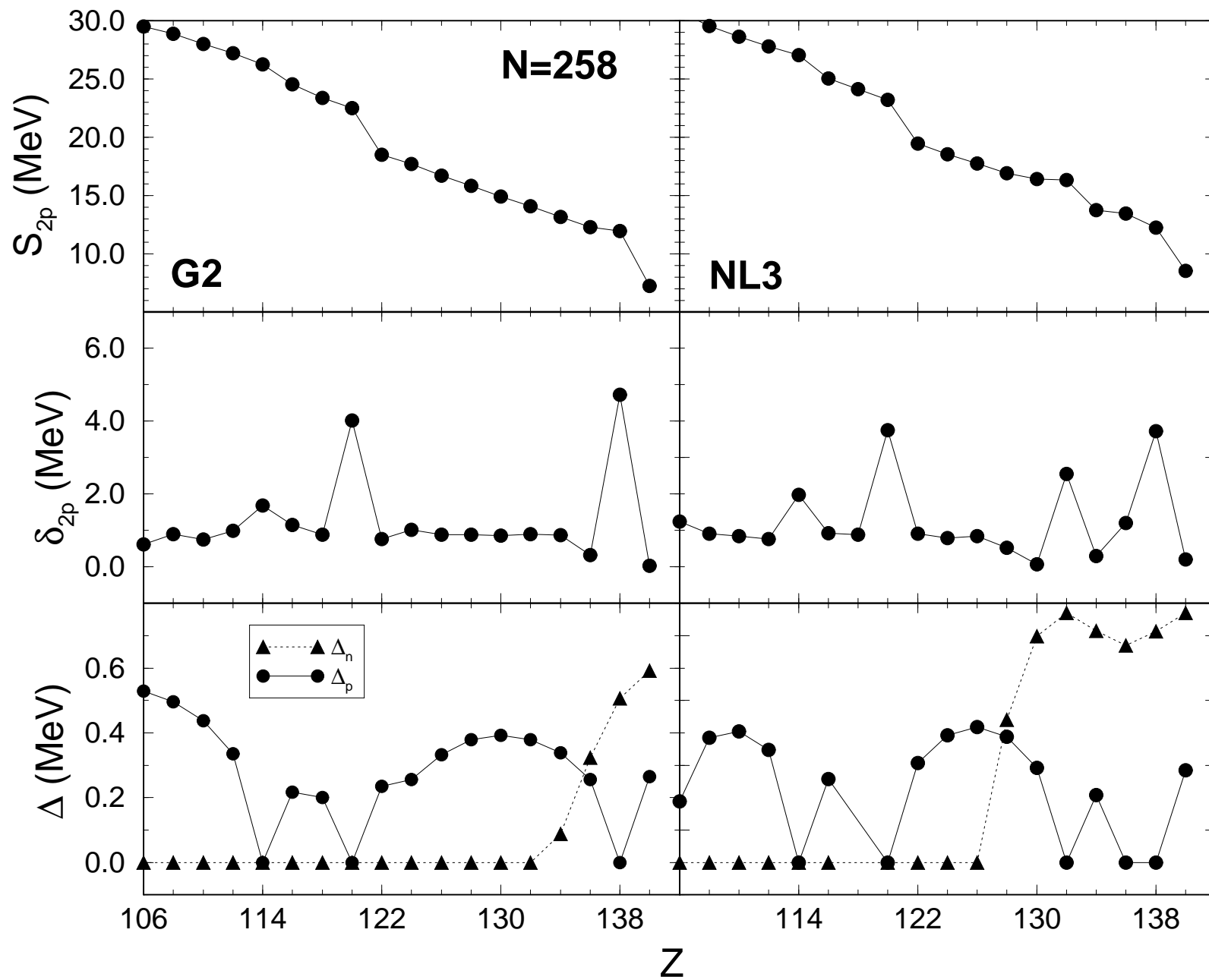


Fig. 8

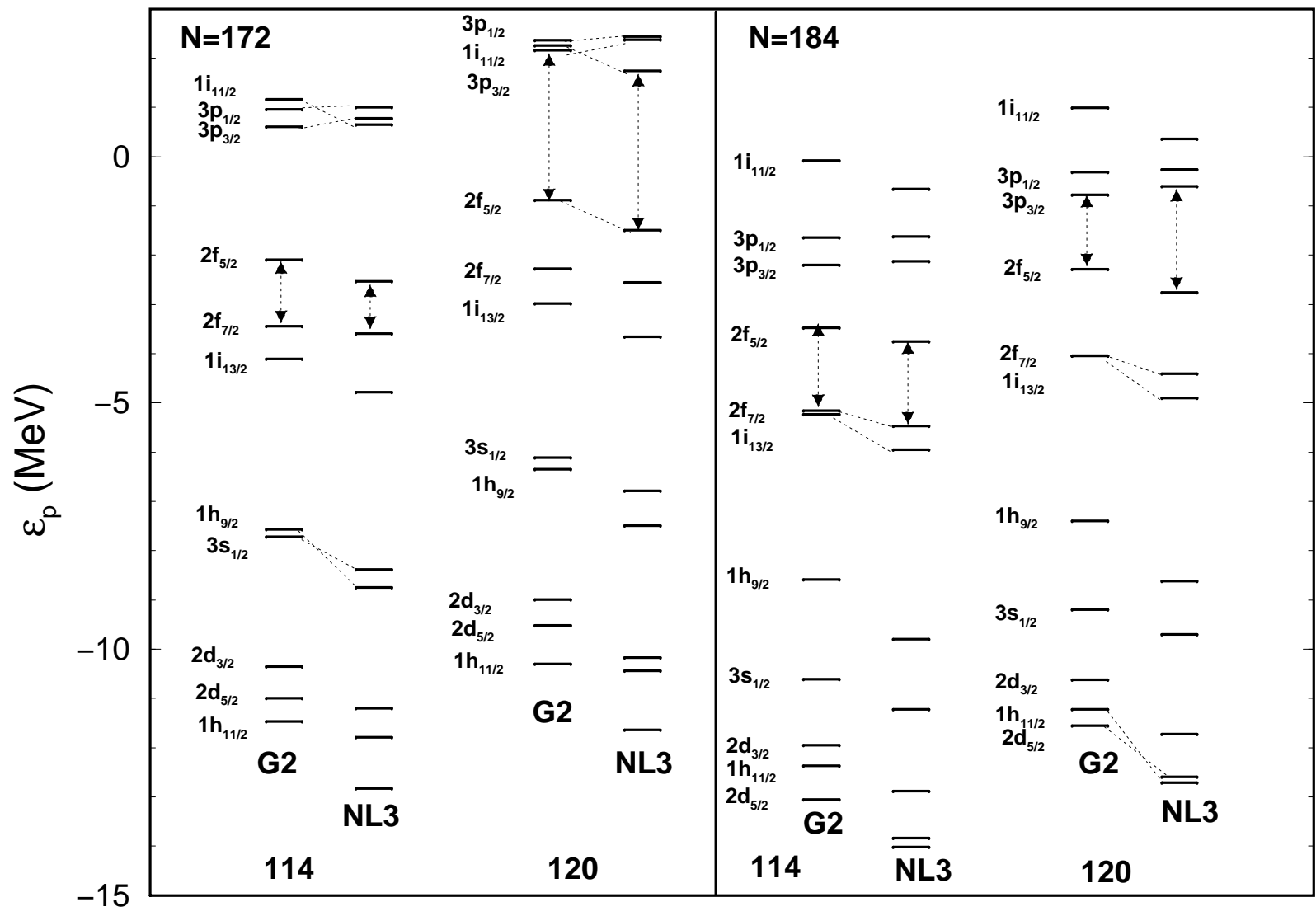


Fig. 9

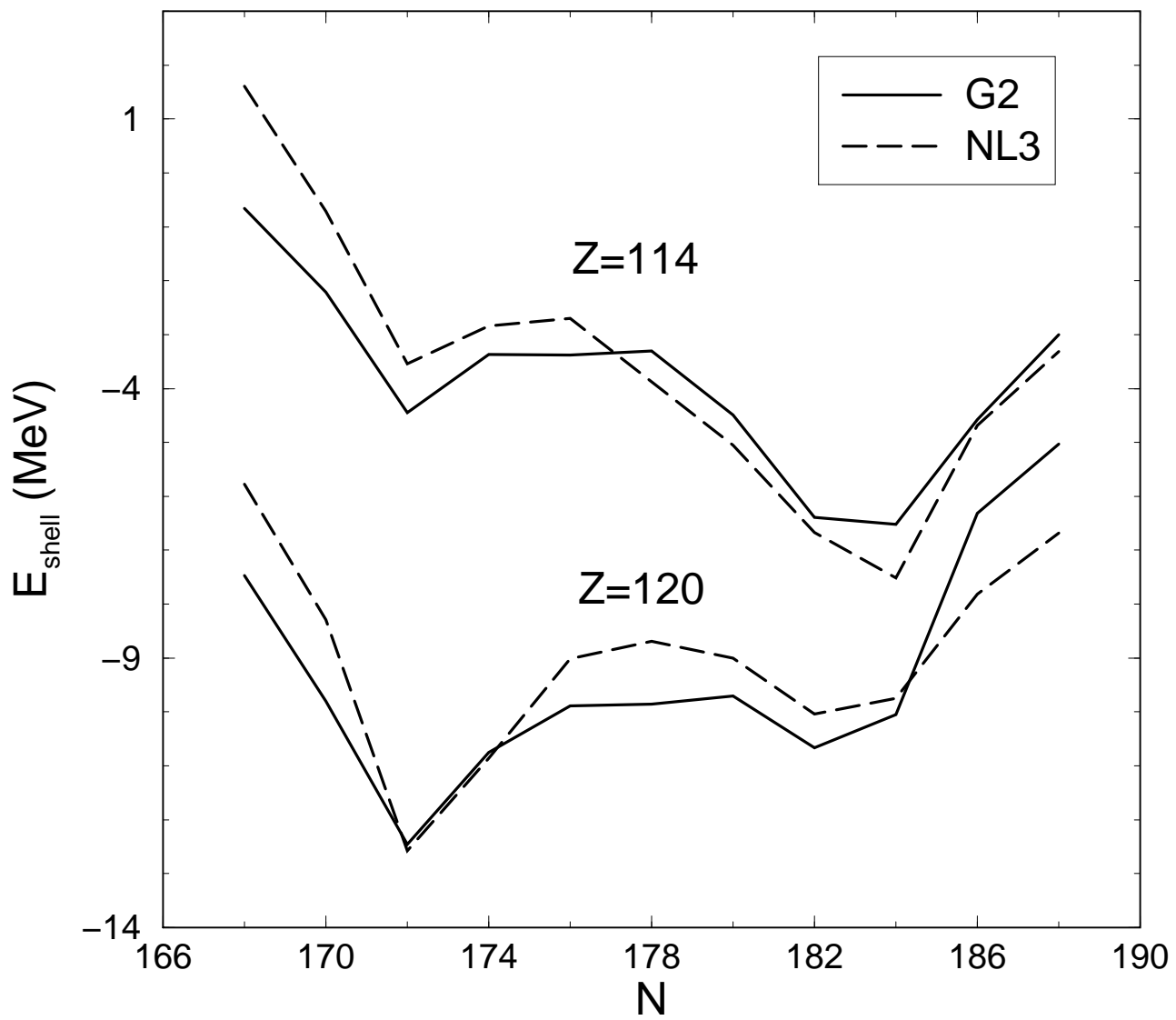


Fig. 10

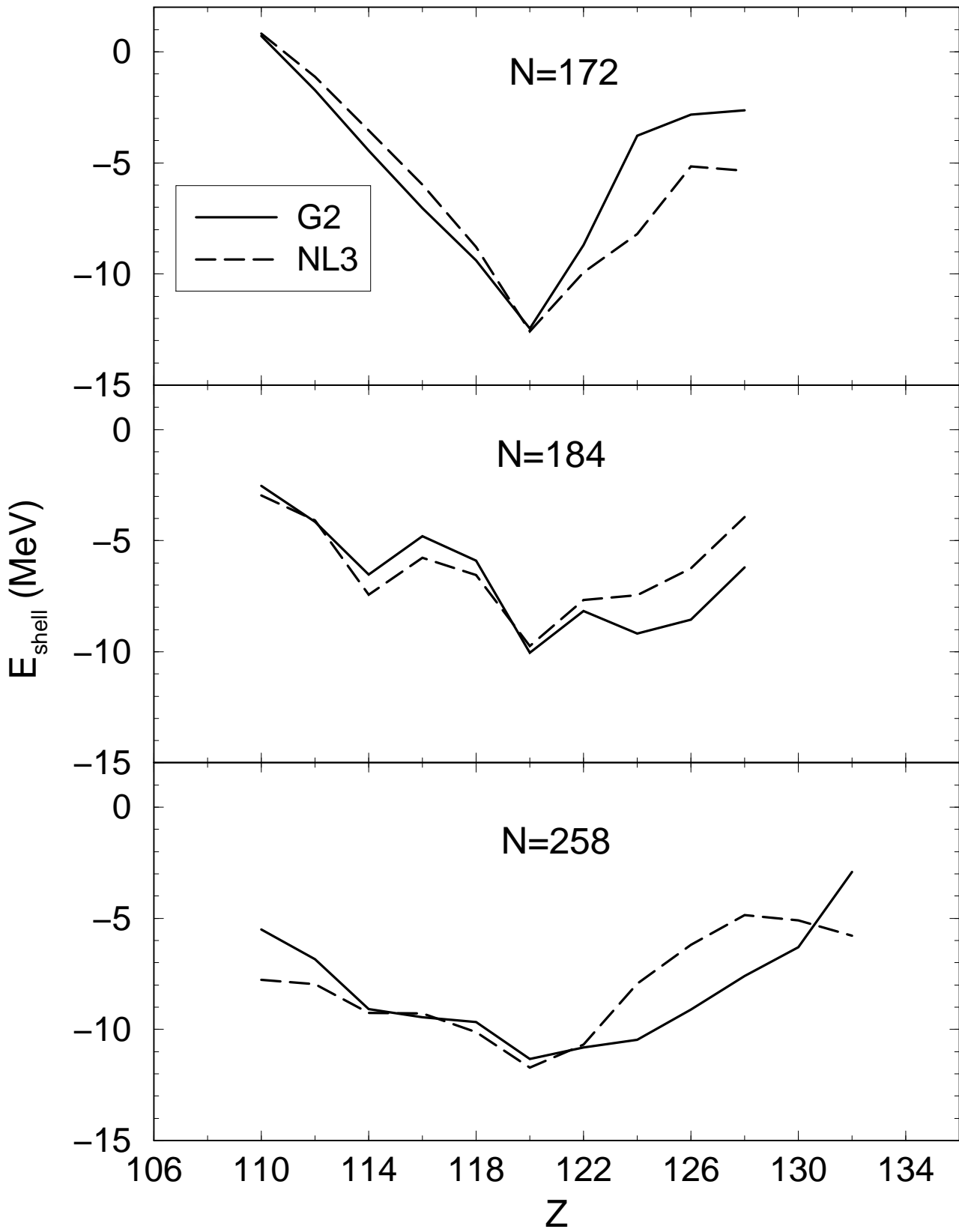


Fig. 11

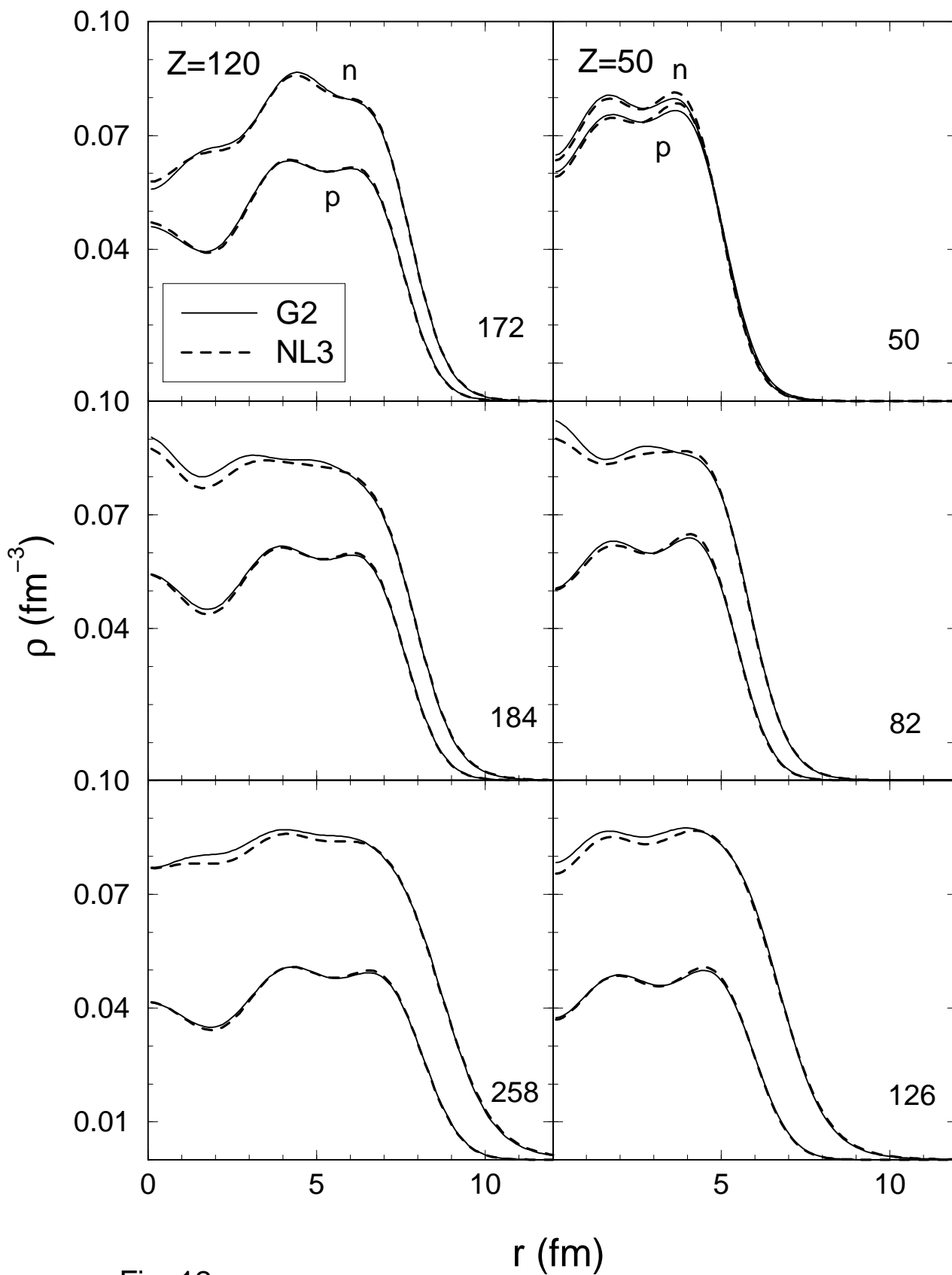


Fig. 12

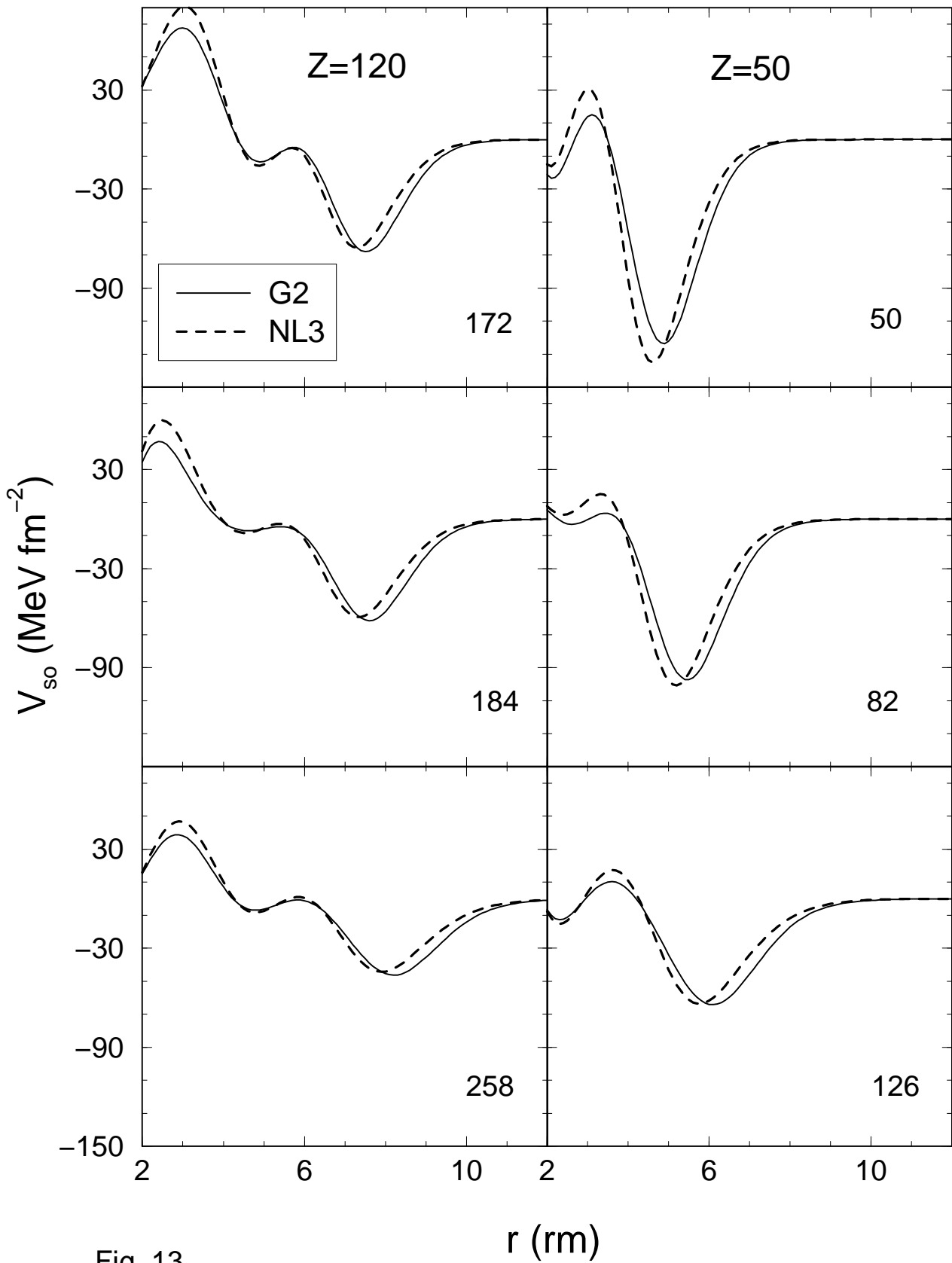


Fig. 13